


Middle Miocene climate transition in the Tibetan Plateau: identification and significance

Shijun Song^{1,2} , Lei Huang^{1,2}, Yongshu Zhang³, Qi Zhang^{1,2}, Fei Zhou³, Chiyang Liu^{1,2}, Yan Chen³, Yingxiong Wu³ and Yiming Zhang^{1,2}

Review Article

Cite this article: Song S, Huang L, Zhang Y, Zhang Q, Zhou F, Liu C, Chen Y, Wu Y, and Zhang Y (2022) Middle Miocene climate transition in the Tibetan Plateau: identification and significance. *Geological Magazine* **159**: 153–172. <https://doi.org/10.1017/S0016756821000893>

Received: 21 November 2020

Revised: 20 July 2021

Accepted: 21 July 2021

First published online: 26 October 2021

Keywords:

fine-grained mixed sediments; Middle Miocene Climatic Optimum (MMCO); Yiliping Depression; Qaidam Basin

Author for correspondence:

Lei Huang,

Email: huanglei@nwu.edu.cn

¹State Key Laboratory of Continental Dynamics, Northwest University, Xi'an, China/Department of Geology, Northwest University, Xi'an, Shaanxi 710069, China; ²Institute of Oil and Gas Basin, Northwest University, Xi'an, China and ³Exploratory Development Institute, Qinghai Oilfield Company, CNPC, Dunhuang, Gansu 73200, China

Abstract

The Middle Miocene Climatic Optimum is known for abrupt events during the global cooling trend of the past 20 Ma. Its identification in the Tibetan Plateau can help explain the cause of the critical Middle Miocene climate transition in Central Asia. In this study, fine-grained mixed sediments widely distributed in the Miocene Qaidam Lake in the northern Tibetan Plateau were used as a sensitive indicator for palaeoclimate. Their geochemical characteristics were investigated, together with an analysis of 2600 m long successive gamma-ray logging data from the whole JS2 drillcore, to understand the mid-Miocene climate transition in the Tibetan Plateau. By comparing the gamma-ray curve of the mixed sediments with global temperature, the Middle Miocene Climatic Optimum event can be easily identified. Further, the detailed petrological features and geochemical data of lacustrine fine-grained mixed sediments from a 400 m drillcore show oxidizing, high-sedimentation rate and brackish-saline water conditions in a semi-arid climate during the Middle Miocene period, demonstrating a dryer climate in the Qaidam Basin than in the monsoon-sensitive regions in Central Asia. These fine-grained mixed sediments have recorded climate drying before 15.3 Ma that represents a climatic transition within the Middle Miocene Climatic Optimum; increasing carbonate-rich mixed sediments, decreasing algal limestone layers and decreasing lacustrine organic matter are indicators of this transition. Regional tectonic events include the retreat of the Paratethys from Central Asia at ~15 Ma and the synchronous tectonic reorganization of the Altyn-Tagh fault system and the northeastern Tibetan Plateau. We find that global climate change is the primary factor affecting the overall characteristics and changes of the Neogene climate in the Qaidam Basin, including the occurrence of the Middle Miocene Climatic Optimum and the cooling and drying tendency, while the regional events are a secondary factor.

1. Introduction

The Middle Miocene climate is an abrupt and dramatic instance of global warming and cooling during the long-term cooling trend of the Cenozoic Era (Savin *et al.* 1975; Flower & Kennett, 1994; Zachos *et al.* 2001; Böhme, 2003). It is characterized by two distinct features: the Middle Miocene Climatic Optimum (MMCO; 17–15 Ma), characterized by annual mean surface temperatures 3–6 °C higher than today (Flower & Kennett, 1994; Zachos *et al.* 2001; Böhme, 2003), and the Middle Miocene Climate Cooling (MMCC; 14.2–13.8 Ma), in which the global average temperature dropped more than 5 °C, a change associated with the formation of the East Antarctic ice sheet, eventually leading to the aridity of the middle- and high-latitude continental interiors, such as inland Asia, Australia, Africa, North America and South America (Retallack, 1992; Flower & Kennett, 1994; Webb, 1997; Holbourn *et al.* 2014). The Middle Miocene is considered the most critical interval, known as ‘the Middle Miocene Climatic Transition’ (Flower & Kennett, 1994; Zachos *et al.* 2001), and represents a transition period from a relatively humid to arid climate. Because the Middle Miocene climate changes were unrelated to human activities, it is a research hotspot (Böhme, 2003). Until now, the MMCO and MMCC events have been widely reconstructed via oxygen isotope records from marine sediments (Flower & Kennett, 1994; Zachos *et al.* 2001; Böhme, 2003).

The Tibetan Plateau experienced a strong uplift during Miocene time that changed the local precipitation patterns (Fang *et al.* 2007; Lu & Xiong, 2009; Miao *et al.* 2011, 2012; Lin *et al.* 2015). This effect made the Middle Miocene climatic transition more complicated in Central Asia; as a result, the cause of this regional climate change, whether global climatic changes or Tibetan Plateau uplift, is difficult to determine. Therefore, the identification and detailed characterization of the critical Middle Miocene climate transition in Central Asia is very important, as it can help us to comprehend this issue. The present investigations of the MMCO and MMCC in Asia mainly come from the humid regions (i.e. the east Asian monsoon region) at the eastern edge of

the Tibetan Plateau (e.g. Hou *et al.* 2014; Lin *et al.* 2015; Zan *et al.* 2015; Lebreton-Anberrée *et al.* 2016; Song *et al.* 2017; Dong *et al.* 2018; Hui *et al.* 2018). Considering that the Tibetan Plateau has expanded towards the north and northeast since the Miocene Epoch (Tapponnier, 2001; Rowley & Currie, 2006), the climate evolution in arid regions close to the interior Tibetan Plateau may supply us with more sensitive information about climate drying and tectonics compared with information from the monsoon-sensitive regions.

The Qaidam Basin is an important petroliferous basin in the Tibetan Plateau that is characterized by fine-grained mixed sediments that developed during the Cenozoic Era (Xiong *et al.* 2018; Xu *et al.* 2018; Yu *et al.* 2018). Mixed sediments are formed by mixing terrigenous clasts and intrabasinal carbonate. They can be deposited in various environments, such as lakes, transitional, shelf and slope facies. The mixing ratio of allogenic and authigenic components in mixed sediments is considered to be significantly influenced by climate and environment (Mount, 1984; Brooks *et al.* 2003; Campbell, 2005; Garcia-Garcia *et al.* 2009; Chiarella *et al.* 2017); thus, they can be used for reconstructing palaeoclimate changes after excluding the interference of tectonics, detrital sources and sedimentary cycles. In this study, we investigate the petrology and geochemistry of mixed sediments from the Qaidam Basin to reconstruct the palaeoclimate and palaeoenvironment during Middle Miocene time. The paper (1) identifies and explains the Middle Miocene climate transition in the Tibetan Plateau, and (2) discusses the driver of climatic change in Central Asia during this period.

2. Geologic setting

The Qaidam Basin, with an average elevation of 2000–3000 m, is the largest intermontane basin at the northern part of the Tibetan Plateau (Fig. 1a). It is surrounded by the Altyn-Tagh Fault, Qilian Mountain and Kunlun Mountain in the northwest, northeast and south, respectively (Tapponnier, 2001; Cowgill *et al.* 2004; Gold *et al.* 2011). The Cenozoic stratigraphy of the Qaidam Basin is divided into seven formations, namely the Lulehe Formation (E_{1+2}), Xianganhaigou Formation (E_3) and Shangganhaigou Formation (N_1), deposited during the Palaeogene Period; and the Xiayoushashan Formation (XYSS Fm; N_2^1), Shangyoushashan Formation (SYSS Fm; N_2^2), Shizigou Formation (SZG Fm; N_2^3) and Qigequan Formation (QGQ Fm; Q_{1+2}), deposited during the Neogene and Quaternary periods (Yang, *et al.* 1992; Sun *et al.* 2004; Lu & Xiong, 2009). During the Neogene Period, owing to the relatively arid palaeoclimate and the high salinity of the lake water, lacustrine fine-grained sedimentary rocks characterized as mixed sedimentary were widely distributed in the Qaidam Basin (Sha, 2001; Xu *et al.* 2014; Xiong *et al.* 2018).

During the Miocene–Pliocene epochs, the depocentre of the Qaidam Basin migrated from west to east owing to the uplift of Kunlun Mountain; consequently, the Yiliping Depression became the long-term depocentre and accumulated very thick lacustrine strata (Guo *et al.* 2009; Fig. 1c). During this period, the SYSS and XYSS fms, composed of shore–shallow lacustrine sedimentary facies (including algal flats, lime-mud flats and beach bar subfacies), were deposited in the Yiliping Depression (Guo *et al.* 2009; Xu *et al.* 2018; Fig. 1b). The lithology of the SYSS and XYSS fms mainly consists of fine-grained sedimentary rocks, such as dark silty mudstone, argillaceous siltstone and marlstone, whereas the lithology of the SZG Fm mainly consists of

light-coloured siltstone and argillaceous siltstone. In addition, the SZG Fm contains white halite and black gypsum interlayers, which are rarely found in the SYSS and XYSS fms (Fig. 1b).

3. Samples and methods

In this study, 148 samples of the XYSS and SYSS fms from seven wells (JS2, FX103, F8, F6, L1, H2, JS1) in the Yiliping Depression were used to determine the rock components, using the Rigaku D/max-2500X X-ray fluorescence spectrometer of the Analytical Centre at the Xi'an Centre of China Geological Survey.

Among these seven wells, the JS2 well is our primary object of study. This well penetrated ~3000 m of Neogene–Quaternary strata, including the QGQ, SZG, SYSS and XYSS fms. In addition, a 400 m successive coring section of the JS2 drillcore was obtained. This coring section contains an 81 m thick segment of the SYSS Fm and a 319 m thick segment of the XYSS Fm. To determine the abundance of major and trace elements, 34 samples from JS2 with an average spacing were analysed using a Philips PW2404 X-ray fluorescence spectrometer and a Perkin-Elmer NexION-300D inductively coupled plasma mass spectrometer, respectively. These analyses were conducted at the Laboratory of Continental Dynamics at Northwest University. In addition, total organic carbon (TOC) concentrations from the JS2 samples were obtained using a Leco CS-200 carbon sulfur analyser at the Organic Geochemistry Laboratory of Exploration and Development Research Institute of PetroChina, Qinghai Oilfield Branch Company. Moreover, 2600 m long successive gamma-ray logging data from this well were used to analyse the long-term climatic change.

4. Results

4.a. Petrological features

Fine-grained sedimentary rocks are dominant in the study area. Owing to their black, dark-grey and brownish-grey colours, they were easily recognized as dark mudstones (Fig. 2a). The X-ray diffraction results indicate that most of the 148 samples mainly contain siliciclastic, carbonate and clay components, with relative contents varying from 20.9 to 48.1 % (mean = 30.5 %), 17.1 to 45.0 % (mean = 34.4 %) and 18.4 to 48.4 % (mean = 35.1 %), respectively (Fig. 2f). According to the classification scheme of fine-grained sedimentary rocks from Jiang *et al.* (2013) and Yan *et al.* (2015), these samples are classified as fine-grained mixed sediments. In addition, some interlayers of algal limestone, with thicknesses ranging from 20 to 100 cm, and stromatolitic structures can be observed (Fig. 2b).

In the 400 m successive coring section of the JS2 drillcore, fine-grained mixed sediments dominate, with intermittent deposits of algal limestone interlayers (Fig. 3). According to the number of algal limestone interlayers, the whole coring section can be divided in two parts: A and B. The number of algal limestone interlayers in section B is clearly more than that in section A. Homogeneous structures and bedding structures can be observed in the fine-grained mixed sediments. The bedding structures include lenticular, veined, wavy bedding and climbing ripple bedding composed of fine sand containing anhydrite (Fig. 2c, d). In some samples from section A (JS2-0174, JS2-0505, JS2-0758 and JS2-0689) with a light colour, tiny lenticles or horizontal strips of gypsum can be observed (Fig. 3). In the algal limestones in section B, the colours are mainly greyish-white or yellowish-grey,

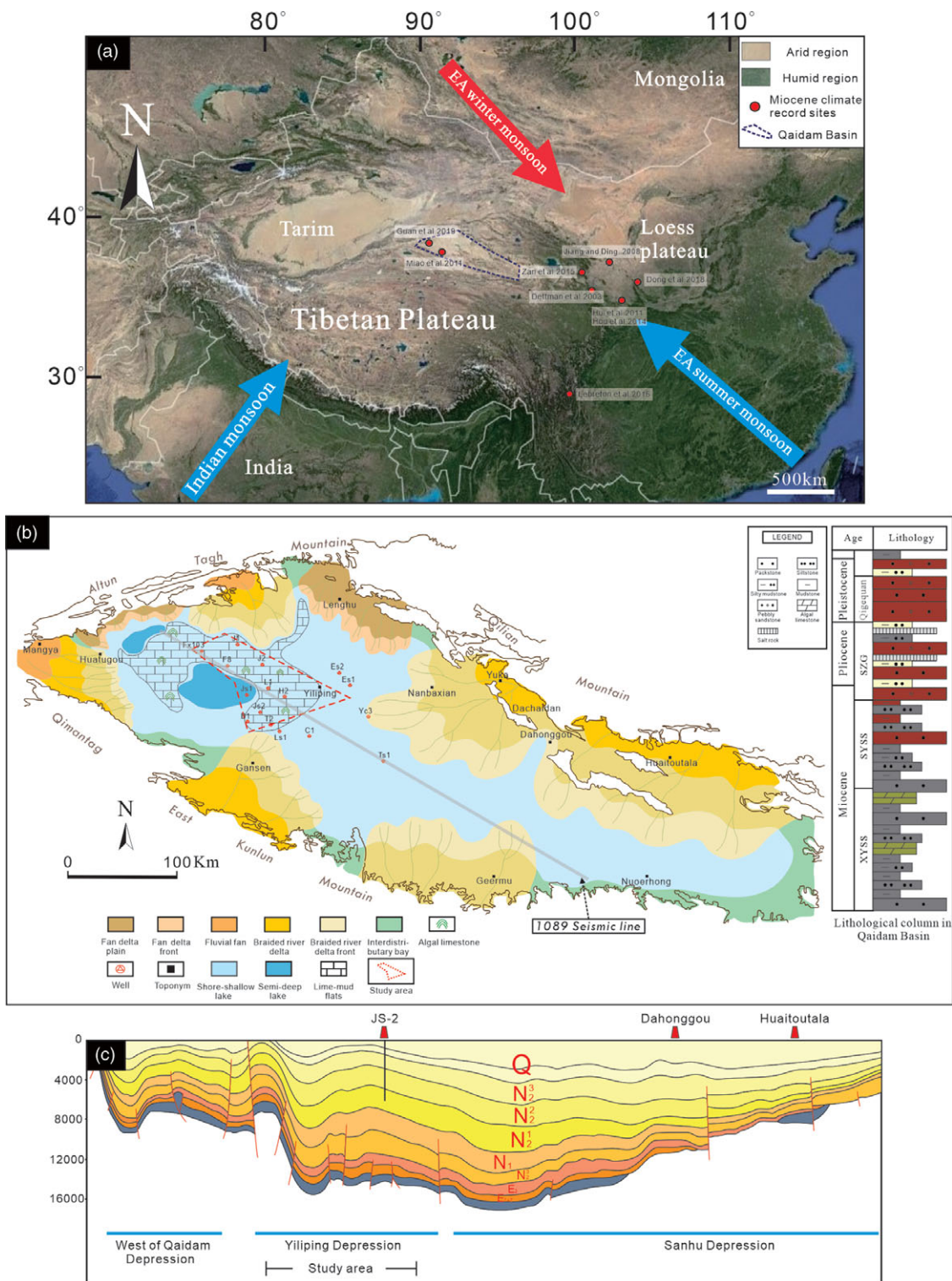


Fig. 1. (Colour online) (a) Satellite map showing the arid and humid regions in Central Asia; the Tibetan Plateau is located in an arid region. (b) The sedimentary facies of the Qaidam Basin during the Miocene Epoch. (c) The 1089 seismic profile shows the west side of the Qaidam Basin Depression, the Yiliping Depression, the Sanhu Depression and the location of the JS2 drillcore. Note that the original data for (b) and (c) come from the Qinghai Oilfield Branch Company in China.

and they have a stromatolitic structure composed of black filaments and white anhydrite laminations (Figs 2b, 3). Furthermore, observations made using a polarized light microscope, electron probe X-ray microanalysis and a scanning electron

microscope indicate that these fine-grained mixed sediments are homogeneous mixing products of clay minerals, silt-sized felsic particles, micritic carbonate grains, tiny anhydrite particles and other substances (Fig. 4a–d).

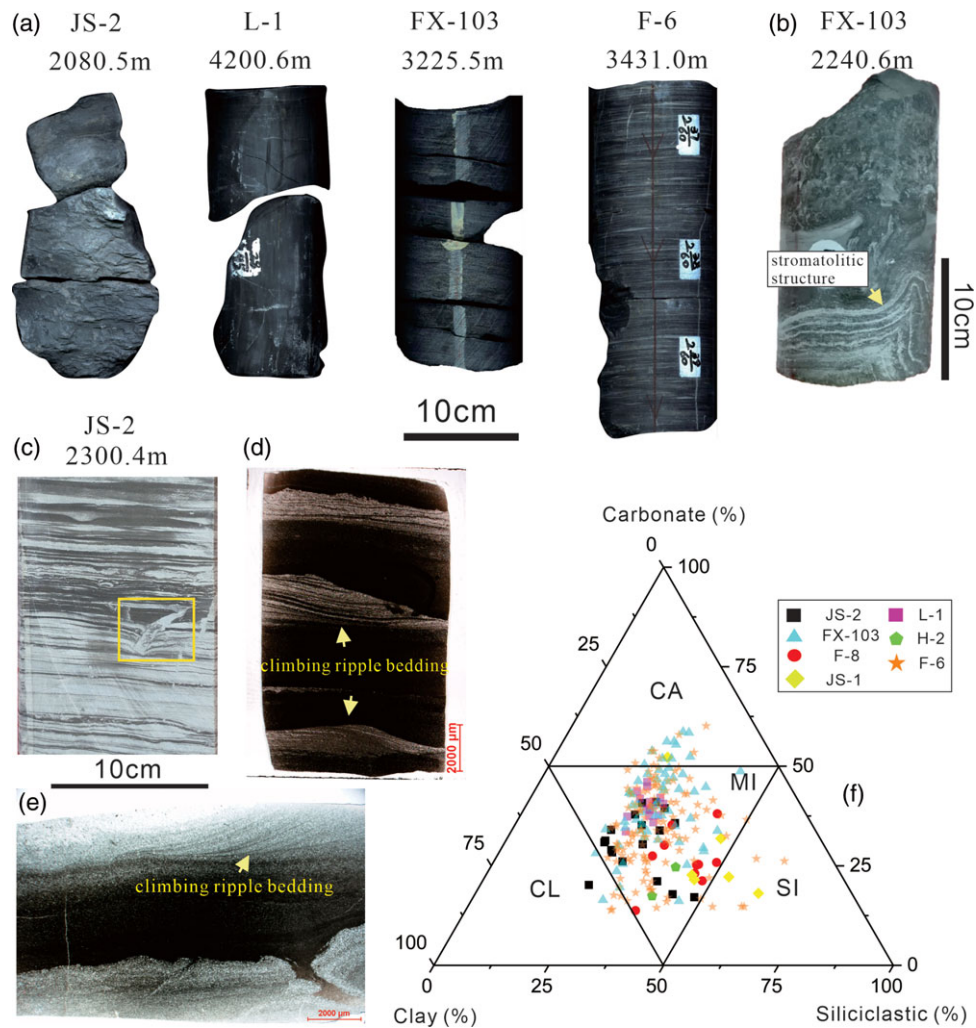


Fig. 2. (Colour online) (a) Macro-features of fine-grained mixed sediments from the JS2, FX103, F6 and L1 drillcores, similar to dark mudstones. (b) Macro-features of algal limestones in the FX103 drillcore, and the black filaments interbedded with white anhydrite lamina. (c) The stratified fine-grained mixed sediments from the JS2 well, and the slump deposit observed in microstratification (yellow box). (d, e) Large-scale thin-section showing the climbing ripple bedding composed of fine sand containing anhydrite in fine-grained mixed sediments. (f) Ternary plot illustrating carbonate, clay and siliciclastic contents of the Neogene fine-grained sedimentary rocks in the study area (based on Yan *et al.* 2015 and Jiang *et al.* 2013). SI – siliciclastic sedimentary rocks; CA – carbonate rocks (dolomite and limestone); CL – clay rocks; MI – fine-grained mixed sediments.

4.b. Geochemical characteristics of the fine-grained mixed sediments

4.b.1. Major elements

The major-element concentrations of the fine-grained mixed sediments from the coring section of the JS2 drillcore are listed in Table 1. The enrichment factor (EF) can be applied to estimate the degree of enrichment of elements in sediments, and it is defined as follows (Roussiez *et al.* 2005): $EF = (X/Al)_{\text{sample}} / (X/Al)_{\text{NASC}}$, where $(X/Al)_{\text{sample}}$ represents the ratio of the content of the element in question against the content of the element Al of the sample in question, and $(X/Al)_{\text{NASC}}$ represents the ratio of the content of the element against the content of Al in the North American Shale Composite (NASC; Gromet *et al.* 1985). An EF value greater than 1 indicates that the elements are enriched, while a value less than 1 reflects that the elements are depleted compared to the NASC. In this study, the elements Ca, Mg, Na and Mn show obvious enrichment, and the element P shows slight enrichment. The elements Si, T, Al and K are comparable with those in the NASC, which have no obvious enrichment or depletion. The elements Ca and Mg are most enriched in the

samples JS2-0174, JS2-0505, JS2-0689, JS2-0111 and JS2-0758 from section A (Table 1; Fig. 5a). Combining this with petrological observations, we find that all the samples are rich in carbonate and gypsum. Based on this, we define these samples (JS2-0174, JS2-0505, JS2-0689, JS2-0111, JS2-0758) as endogenous or carbonate-rich fine-grained mixed sediments, and the other samples can be regarded as exogenous fine-grained mixed sediments.

4.b.2. Trace elements

Trace-element concentrations of the fine-grained mixed sediments from the coring section of the JS2 well are listed in Table 2. Ba (326.0–1290.5 ppm, mean = 505.0 ppm), Sr (224.0–2638.9 ppm, mean = 649.4 ppm), Zr (91.0–212.7 ppm, mean = 142.0 ppm) and Rb (62.2–145.9 ppm, mean = 110.6 ppm) are the most abundant elements. Some trace-element EFs for the fine-grained mixed sediments are shown in Figure 5b: Sc (EF = 1.12–1.26, mean = 1.18), Rb (EF = 1.07–1.27, mean = 1.18), Sr (EF = 1.76–31.44, mean = 7.73), Cs (EF = 1.84–2.82, mean = 2.48), Ba (EF = 0.78–3.34, mean = 1.17), Th (EF = 1.03–1.64, mean = 1.42) and U (EF = 1.31–3.55, mean = 2.05) have an average EF higher

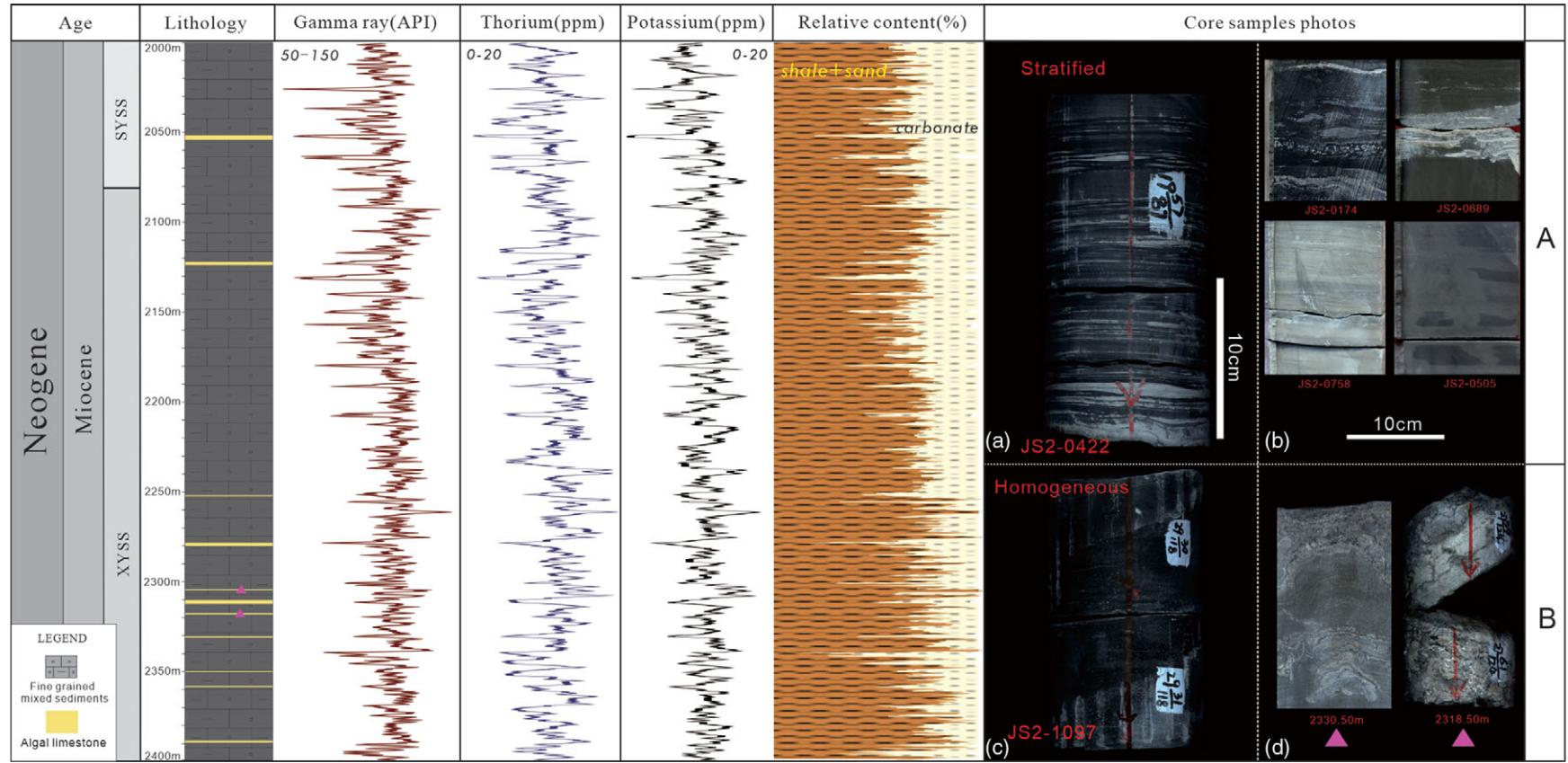


Fig. 3. (Colour online) Lithological column from the coring section of the JS2 drillcore in the Yiliping Depression showing fine-grained mixed sediments and algal limestone interlayers. Note that, according to the number of algal limestone interlayers, this section is divided in two, A and B. (a) Core photographs show the normal fine-grained mixed sediments from section A, which are similar in appearance to dark mudstones. (b) Core photographs illustrate the abnormal fine-grained mixed sediments from section A, which are clearly different in appearance from the normal fine-grained mixed sediments. (c) Core photographs show the normal fine-grained mixed sediments from section B, which have no obvious difference from that in section A. (d) Core photographs show algal limestones and their stromatolitic structure from section B.

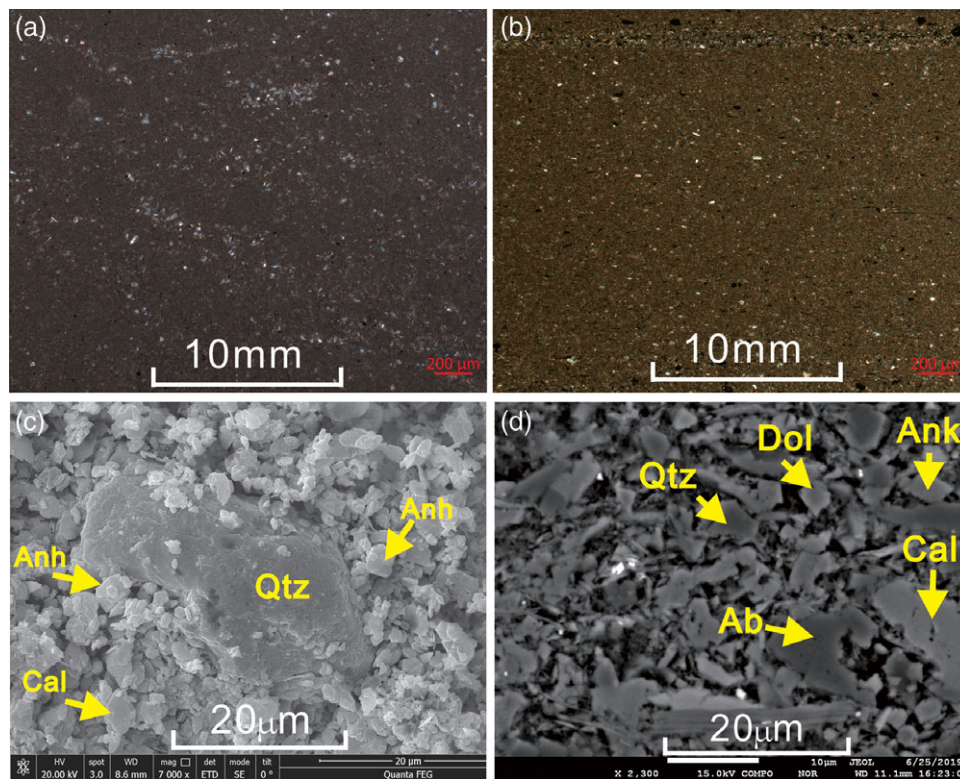


Fig. 4. (Colour online) Microscopic features of fine-grained mixed sediments in the Yiliping Depression. (a, b) Polarizing photomicrograph showing micrite, clay and silt mixed together in the fine-grained mixed sediments. It is difficult to directly estimate the relative contents of them. (c) Electron probe photomicrograph showing anhydrite (Anh), calcite (Cal) and quartz (Qtz) mixed together in a state of dispersive particles from the JS2 well. (d) Scanning electron photomicrograph showing quartz (Qtz), calcite (Cal), dolomite (Dol), ankerite (Ank) and albite (Ab) mixed together in the JS2 well, with particle size less than 30 μm.

than 1. Among them, Sr shows obvious enrichment, especially in the endogenous mixed sediments from section A.

4.b.3. Rare earth elements

The results of the rare earth element (REE) analysis of the fine-grained mixed sediments are listed in Table 3. The values of total rare earth elements (Σ REEs) of the exogenous fine-grained mixed sediments vary from 124.7 to 176.9 ppm, with an average of 156.5 ppm; these values are lower than those for Post-Archaean Australian Shale (PAAS; 183.0 ppm; Taylor & McLennan, 1985), but approximate to the NASC (167.4 ppm; Gromet *et al.* 1985). The Σ REEs of the endogenous mixed sediments vary from 88.6 to 123.7 ppm, with an average of 107.9 ppm. The distribution pattern of REEs in the fine-grained mixed sediments is unified and shows a trend of from high to low from left to right, close to the NASC and PAAS (Fig. 8a).

4.b.4. Data validity analysis

Geochemical data have been widely used to trace the provenance and reconstruct the palaeoclimate and palaeoenvironment (Shields & Stille, 2001; Tribouillard *et al.* 2006). However, a precondition of the reconstruction is that the elements must represent the synsedimentary characteristics of sediments and not be affected by late diagenesis or detrital input (Tribouillard *et al.* 2006). As a portion of the components in the mixed sediments is of detrital provenance, validity analysis of their geochemical data is particularly important. Generally, if an element is not mainly of detrital provenance, it can be used for palaeoenvironmental analysis; by contrast, if an element is mainly detrital, it can be used for the analysis of provenance information (Tribouillard *et al.* 2006).

A reliable means to determine whether the content of a given element is controlled by detrital input is to cross-plot the trace and major elements versus Al, which is commonly of detrital origin and usually stable during diagenesis (Tribouillard *et al.* 1994; Böning *et al.* 2004). The correlations of major, trace and REEs from 34 samples are shown in Figure 6. The contents of V, U, Co, Na₂O, K₂O, Th, Cu, Sc, La and Σ REEs are positively correlated with that of Al₂O₃, suggesting that these elements were mainly from terrestrial sources and can be used to reflect the provenance (Tribouillard *et al.* 2006). In particular, a strong positive correlation between Σ REEs and Al₂O₃ indicates that the REEs in the fine-grained mixed sediments were not affected by post-depositional diagenesis (Shields & Stille, 2001).

As mentioned above, for carbonate components in mixed sediments, usually only the authigenic ones can be used to recover estimates of the palaeoclimate and palaeoenvironment. We suggest that the carbonate components in the mixed sediments studied here are mainly authigenic. This claim is supported by the following points. First, for carbonate grains in a lake basin, intraclasts are usually micritic carbonate grains and extraclasts are polycrystalline marble grains (Rieser *et al.* 2005); these observations were made using a scanning electron microscope and indicate that lacustrine carbonates from the fine-grained mixed sediments are almost all micritic grains in the Yiliping Depression (Fig. 4). Second, the mixed sediments of the Yiliping Depression (the contents of CaO and MgO, which represent calcite and dolomite, respectively) have a negative correlation with that of Al₂O₃, indicating that most carbonate in the fine-grained mixed sediments is authigenic; moreover, the contents of Sr and Ba are also negatively correlated with that of Al₂O₃, indicating that the elements Sr and

Table 1. V_{co} , major-element abundances and some associated parameters of fine-grained mixed sediments from the coring section (unit in %)

Samples	Depth (m)	SiO ₂	TiO ₂	Al ₂ O ₃	TFe ₂ O ₃	MnO	MgO	CaO	Na ₂ O	K ₂ O	P ₂ O ₅	LOI	Total	CIA
JS2-0003	2001.0	49.4	0.6	13.5	5.2	0.1	3.3	10.4	2.2	2.8	0.2	11.9	99.5	57
JS2-0019	2006.1	51.0	0.6	15.2	5.9	0.1	3.3	7.6	2.2	3.2	0.1	10.2	99.5	58
JS2-0096	2029.1	47.2	0.6	13.5	5.2	0.1	3.1	11.6	2.9	2.9	0.2	12.7	99.8	52
JS2-0128	2040.1	46.8	0.6	12.7	5.0	0.1	3.2	13.0	2.0	2.7	0.2	13.4	99.5	58
JS2-0216	2069.0	48.0	0.6	14.4	5.5	0.1	3.6	10.2	2.2	3.1	0.1	12.0	99.7	58
JS2-0246	2079.7	48.8	0.6	15.6	6.1	0.1	4.2	7.4	2.2	3.4	0.1	11.2	99.6	59
JS2-0277	2089.4	53.5	0.5	10.0	3.3	0.1	2.6	12.5	2.5	1.9	0.1	12.6	99.6	49
JS2-0309	2099.1	50.7	0.6	14.5	5.6	0.1	3.4	8.5	2.1	3.1	0.2	11.0	99.8	59
JS2-0325	2103.9	40.8	0.5	11.5	4.5	0.1	3.8	16.3	1.9	2.4	0.1	17.6	99.5	57
JS2-0367	2119.1	52.9	0.7	14.2	5.2	0.1	3.1	8.0	2.3	3.0	0.2	10.2	99.7	57
JS2-0403	2128.9	42.7	0.6	13.4	5.5	0.1	4.2	13.8	1.8	2.8	0.1	14.7	99.7	60
JS2-0422	2133.8	47.5	0.6	12.6	4.9	0.1	4.5	11.2	2.0	2.6	0.2	13.5	99.7	57
JS2-0489	2153.5	48.5	0.6	10.7	4.2	0.1	2.5	14.9	2.2	2.1	0.1	13.9	99.7	53
JS2-0551	2173.4	45.6	0.6	12.3	4.8	0.1	3.4	13.8	2.0	2.6	0.1	14.4	99.7	57
JS2-0622	2192.4	52.2	0.6	13.9	4.8	0.1	2.9	8.8	2.5	2.9	0.1	10.7	99.5	55
JS2-0706	2217.6	47.2	0.6	12.4	4.5	0.1	3.0	13.4	2.0	2.6	0.1	14.0	99.8	57
JS2-0741	2227.7	50.1	0.6	13.2	5.1	0.1	3.5	10.4	2.2	2.7	0.2	11.6	99.6	57
JS2-0830	2252.7	40.7	0.5	11.1	5.0	0.1	4.5	16.6	1.9	2.2	0.1	17.1	99.8	56
JS2-0871	2262.8	49.6	0.6	14.4	5.3	0.1	3.2	9.9	2.0	3.1	0.2	11.3	99.7	59
JS2-0905	2272.9	49.8	0.6	14.7	5.7	0.1	3.3	9.6	2.0	3.1	0.2	11.1	100.0	60
JS2-0957	2287.3	49.5	0.6	13.3	5.0	0.1	3.5	10.6	2.1	2.8	0.2	12.0	99.6	58
JS2-0972	2292.4	42.5	0.5	13.0	5.4	0.1	3.4	14.7	1.9	2.7	0.1	15.4	99.6	59
JS2-1097	2327.2	45.0	0.6	13.1	5.3	0.1	3.3	13.6	1.9	2.7	0.1	13.9	99.5	59
JS2-1154	2342.5	48.1	0.6	13.6	5.3	0.1	3.4	11.4	2.1	2.8	0.2	12.4	99.8	58
JS2-1183	2352.6	47.2	0.6	12.3	4.9	0.1	2.5	14.2	2.0	2.5	0.1	13.2	99.5	57
JS2-1228	2367.5	49.6	0.5	10.0	3.2	0.1	2.0	15.8	2.1	2.0	0.1	14.4	99.7	53
JS2-1245	2372.6	47.7	0.6	15.2	6.3	0.1	3.7	9.0	2.1	3.2	0.1	11.7	99.6	60
JS2-1283	2387.5	52.6	0.7	15.4	5.6	0.1	3.4	6.8	2.3	3.3	0.1	9.9	100.0	59
JS2-1318	2397.4	42.2	0.5	13.0	5.6	0.1	3.2	14.5	2.1	2.7	0.1	14.5	98.5	57
JS2-0111*	2034.1	34.9	0.5	9.1	4.4	0.1	8.2	16.1	1.8	1.9	0.1	21.8	98.9	54
JS2-0174*	2054.1	22.1	0.3	6.8	3.3	0.1	3.9	28.3	1.1	1.4	0.1	20.2	87.6	57
JS2-0505*	2158.7	28.0	0.4	8.9	4.2	0.1	5.0	24.2	1.6	1.9	0.2	25.2	99.7	55
JS2-0689*	2212.7	29.7	0.4	8.2	4.0	0.1	4.2	25.1	1.6	1.6	0.1	23.4	98.4	54
JS2-0758*	2232.6	30.9	0.4	10.0	4.3	0.1	10.0	16.6	1.5	2.1	0.2	23.5	99.5	58

*Samples JS2-0111, JS2-0174, JS2-0505, JS2-0689 and JS2-0758 are endogenous fine-grained mixed sediments.

Ba are related to the authigenic process and can be directly used to reconstruct the palaeoenvironment (Tribouillard *et al.* 2006; Wang *et al.* 2021).

Third, numerous studies have suggested that the carbonate of the fine-grained mixed sediments deposited in the Cenozoic Qaidam Lake was authigenic (Xu *et al.* 2014, 2018; Xiong *et al.* 2018) and is characterized by micritic grains deposited in the fine-grained mixed sediments. Fourth, Cenozoic lacustrine carbonates were widely deposited in several basins of the

Tibetan Plateau and were considered to be authigenic (e.g. Rowley & Currie, 2006; Zhuang *et al.* 2011; Hou *et al.* 2014). For example, in the Lunpola Basin, located in the central Tibetan Plateau, oxygen isotope data from authigenic lacustrine carbonates were used to estimate the palaeo-elevation of the plateau. Fifth, lacustrine carbonate was a typical and important component in saline lacustrine basins, such as the Jiangnan Basin, Bohaiwan Basin and Qaidam Basin in China (Huang & Hinnov, 2014, 2019; Wu *et al.* 2016; Xu *et al.* 2018).

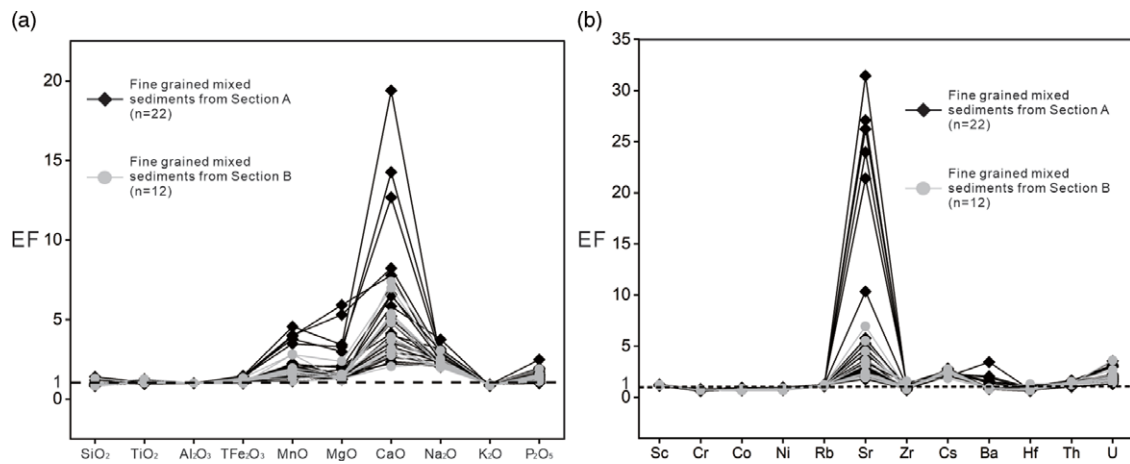


Fig. 5. (Colour online) Enrichment factors (EF) of (a) major elements and (b) some trace elements in fine-grained mixed sediments from the coring section of the JS2 drillcore.

5. Interpretations

5.a. Provenance

The linear relationship of Th/Sc and Zr/Sc indicates that the sedimentary recirculation of the fine-grained mixed sediments is weak, and only a small fraction comes from ancient sediments (Fig. 7a). In general, low TiO_2/Zr ratios (<55) indicate that the source rock is felsic igneous rock; medium TiO_2/Zr ratios (55–200) imply intermediate rock (Hayashi *et al.* 1997); and high TiO_2/Zr ratios (>200) reflect mafic rock (Moradi *et al.* 2016). TiO_2/Zr ratios in the fine-grained mixed sediments range from 27.5 to 50.1, with an average of 39.6, indicating that the source rock is felsic igneous rock, consistent with the result for Co/Th versus La/Sc (Fig. 7b, c). Moreover, in the La–Th–Sc diagram, the data points fall within the continental island arc field, indicating that the tectonic attribution of provenance is a continental island arc source (Fig. 7d). The northern Tibetan Plateau was located in a multi-island arc environment at the edge of the Tethys Ocean as early as the early Palaeozoic period (Xu *et al.* 2006), and the granite scattered around the Qaidam Basin is the potential source rock.

We collected the REE data for granite from Altn-Tagh Mountain, the East Kunlun Mountains and the northern Qaidam Basin and compared their average distribution patterns with that of the fine-grained mixed sediments studied here. Although the REE distribution pattern of the fine-grained mixed sediments is most similar to that of Ordovician granite from the southern portion of Altn-Tagh Mountain, it is completely different from that of the northern section (Fig. 8b). Moreover, the REE distribution pattern of the fine-grained mixed sediments is similar to that of Silurian granite in Qimantag Mountain, but is different from that of Triassic granite in this area and Palaeozoic granites in the northern Qaidam Basin (Fig. 8c, d). On the whole, the source rocks of the fine-grained mixed sediments are Palaeozoic granites, which are widespread in the southwestern basin. Although the ΣREEs of the endogenous fine-grained mixed sediments is clearly lower than that of the exogenous fine-grained mixed sediments, the distribution patterns are consistent, indicating that provenance does not change during their deposition.

5.b. Palaeosalinity, palaeoredox and sedimentation rate

High authigenic Sr content in lacustrine sediments indicates an arid climate (Zhang *et al.* 2004). A Sr/Ba ratio higher than 1 points

to saline water conditions, and ranges from 0.5 to 1 point to brackish water conditions; those lower than 0.5 indicate fresh water conditions (Wang & Wu, 1983; Zheng & Liu, 1999). In this study, the Sr/Ba ratios of the exogenous fine-grained mixed sediments reveal brackish water conditions, whereas the Sr/Ba ratios of the endogenous fine-grained mixed sediments in section A show high values, indicating saline water conditions (Table 2; Fig. 9).

Considering the complex composition of the fine-grained mixed sediments and that their ΣREE values approach those of the NASC, the element values from the NASC can be used to eliminate the interference of terrestrial sources via the following method (Reitz *et al.* 2004; Tribouillard *et al.* 2006): $X_{\text{clastic}} = (X/\text{Al})_{\text{NASC}} \times \text{Al}_{\text{sample}}$, and $X_{\text{authigenic}} = X_{\text{Total}} - X_{\text{clastic}}$. Judging from the calculation results, the elements Co, V, Cr and Ni are nearly all from terrestrial sources, while the contents of authigenic Th and U are 0.24–5.40 ppm and 0.49–5.35 ppm, respectively. Therefore, in this study, the U/Th ratios and authigenic U (U_{aut}) are reliable for reconstructing the redox conditions. It has been widely accepted that U/Th ratios lower than 0.75 point to oxidizing conditions, those from 0.75 to 1.25 point to dysoxic conditions, and those higher than 1.25 indicate anoxic conditions. Meanwhile, U_{aut} values lower than 5 suggest oxidizing conditions, and those higher than 5 point to anoxic conditions (Hatch & Leventhal, 1992; Jones *et al.* 1994). The U/Th ratios (0.23–2.05) and U_{aut} values (0.49–5.35) of the fine-grained mixed sediments in this study reveal oxidizing conditions (Fig. 9; Table 2).

The degree of REE fractionation, namely, La_N/Yb_N (the subscript N represents the NASC, normalized), is generally used to estimate the sedimentation rate in fine-grained sedimentary rocks. It is suggested that a weak REE fractionation results from a high sedimentation rate (La_N/Yb_N ratios ≈ 1 ; Tenger *et al.* 2006; Fu *et al.* 2015). Thus, the high La_N/Yb_N ratios (1.10–1.36, mean = 1.20) of the fine-grained mixed sediments in the study area indicate a high sedimentation rate (Fig. 9; Table 3). The sedimentation rate demonstrates no obvious change from section A to B, also indicating a stable provenance.

5.c. Palaeoclimate as indicated by the geochemical index and petrology characteristics

The Yiliping Depression, as the depocentre of the Qaidam Basin in the Miocene period, accumulated successive lacustrine sediments, with few effects caused by geomorphological change, tectonics and

Table 2. Trace-element contents of fine-grained mixed sediments from the coring section (concentrations in ppm)

Samples	JS2-0003	JS2-0019	JS2-0096	JS2-0128	JS2-0216	JS2-0246	JS2-0277	JS2-0309	JS2-0325	JS2-0367	JS2-0403	JS2-0422	JS2-0489	JS2-0551	JS2-0622	JS2-0706	JS2-0741
Depth (m)	2001.0	2006.1	2029.1	2040.1	2069.0	2079.7	2089.4	2099.1	2103.9	2119.1	2128.9	2133.8	2153.5	2173.4	2192.4	2217.6	2227.7
Li	57.9	63.9	58.3	60.1	67.2	73.6	31.8	58.3	50.0	58.0	68.3	54.1	39.7	53.8	54.8	48.8	59.3
Be	2.3	2.6	2.3	2.2	2.6	2.9	1.5	2.5	2.0	2.5	2.5	2.3	1.7	2.1	2.4	2.1	2.3
Sc	14.5	15.6	14.4	13.3	15.2	16.5	9.8	14.6	12.0	15.0	14.2	13.2	11.0	13.0	14.7	12.7	14.5
V	99.6	112.2	100.1	91.0	107.8	121.8	59.7	101.9	85.3	103.8	102.6	91.6	71.1	89.6	100.7	86.1	98.1
Cr	73.0	81.2	71.8	66.0	75.2	83.3	44.7	72.5	60.2	75.6	72.1	65.6	55.7	66.8	74.0	63.6	74.8
Co	15.6	19.4	16.1	15.4	16.6	18.0	11.8	14.9	12.9	16.1	17.7	14.5	14.4	13.8	14.9	12.5	15.7
Ni	38.5	46.0	35.9	35.7	40.1	44.8	28.2	35.8	30.5	38.2	43.0	33.7	31.5	35.3	37.2	30.1	37.7
Cu	32.9	51.3	32.7	34.2	35.4	43.4	20.9	32.4	25.3	34.0	37.5	30.9	24.4	30.4	34.6	32.0	31.7
Zn	115.9	93.8	119.6	63.8	114.6	86.7	40.8	88.1	56.0	71.0	71.7	73.9	49.7	62.2	70.1	60.1	67.8
Ga	18.6	22.4	18.5	16.6	20.9	23.9	12.0	20.3	15.4	19.5	18.2	16.8	13.5	16.5	19.1	17.0	18.5
Ge	1.5	1.6	1.5	1.3	1.5	1.8	1.1	1.5	1.2	1.6	1.5	1.4	1.2	1.4	1.6	1.4	1.2
Rb	119.0	136.8	123.5	113.8	132.0	145.9	78.9	126.8	106.0	126.8	123.3	110.0	87.9	112.2	126.4	111.4	118.8
Sr	299.7	224.0	249.5	296.1	352.3	482.0	2638.9	267.6	556.7	231.0	287.0	454.3	471.2	1072.2	257.5	315.0	375.4
Zr	173.2	149.8	147.3	153.6	130.0	127.7	102.7	156.8	112.6	179.4	115.2	161.3	152.2	152.2	149.1	133.4	212.7
Nb	14.0	13.7	13.3	13.3	13.2	14.0	10.3	13.5	11.3	14.4	12.4	12.8	12.2	12.2	13.7	12.0	14.3
Cs	10.4	12.6	10.3	9.7	11.6	13.4	6.2	10.6	9.3	10.6	11.5	9.9	6.8	9.4	10.9	9.0	10.3
Ba	453.2	458.0	701.5	420.2	465.8	534.0	1290.5	452.0	397.4	447.7	399.1	470.3	409.6	740.5	437.6	439.3	440.9
Hf	4.6	4.1	4.0	4.2	3.5	3.5	2.7	4.1	3.0	4.7	3.1	4.3	4.0	3.9	3.9	3.5	5.5
Ta	1.0	1.0	1.0	1.0	1.0	1.1	0.8	1.0	0.8	1.1	0.9	1.0	0.9	0.9	1.0	0.9	1.0
Pb	23.6	37.4	21.4	23.7	21.8	22.4	20.2	18.8	16.7	20.5	25.6	20.4	21.4	20.2	18.9	13.7	18.5
Th	15.0	15.6	14.4	14.6	14.5	15.9	7.5	14.3	12.0	15.2	14.6	13.9	10.8	12.6	14.2	12.0	14.9
U	3.9	4.2	3.6	4.2	3.5	4.3	2.1	3.3	4.1	3.4	4.4	3.9	3.4	3.7	3.6	3.5	4.4
Sr/Ba	0.7	0.5	0.4	0.7	0.8	0.9	2.0	0.6	1.4	0.5	0.7	1.0	1.2	1.5	0.6	0.7	0.9
U_{auth}	1.8	1.8	1.5	2.2	1.3	1.9	0.5	1.0	2.3	1.1	2.3	1.9	1.8	1.8	1.4	1.5	2.3
U/Th	0.3	0.4	0.3	0.4	0.3	0.4	2.1	0.3	0.6	0.2	0.5	0.4	0.6	0.5	0.4	0.5	0.4
Samples	JS2-0830	JS2-0871	JS2-0905	JS2-0957	JS2-0972	JS2-1097	JS2-1154	JS2-1183	JS2-1228	JS2-1245	JS2-1283	JS2-1318	JS2-0111*	JS2-0174*	JS2-0505*	JS2-0689*	JS2-0758*
Depth (m)	2252.7	2262.8	2272.9	2287.3	2292.4	2327.2	2342.5	2352.6	2367.5	2372.6	2387.5	2397.4	2034.1	2054.1	2158.7	2212.7	2232.6
Li	47.2	58.1	58.9	53.5	55.3	55.7	61.6	45.7	35.7	65.7	64.0	55.7	43.7	35.1	44.0	32.7	42.6
Be	1.9	2.5	2.6	2.3	2.3	2.2	2.5	2.0	1.7	2.7	2.8	2.1	1.8	1.3	1.7	1.4	1.9

(Continued)

Table 2. (Continued)

Samples	JS2-0830	JS2-0871	JS2-0905	JS2-0957	JS2-0972	JS2-1097	JS2-1154	JS2-1183	JS2-1228	JS2-1245	JS2-1283	JS2-1318	JS2-0111*	JS2-0174*	JS2-0505*	JS2-0689*	JS2-0758*
Sc	11.3	15.0	15.0	13.6	13.4	13.2	14.6	13.2	10.2	16.1	16.1	14.1	10.1	7.4	9.4	8.1	9.9
V	76.8	103.6	103.4	95.4	96.0	93.6	98.7	81.4	65.5	115.5	114.9	105.4	68.3	55.5	70.6	58.0	74.5
Cr	57.6	77.1	75.5	71.8	69.2	68.8	73.2	60.3	50.2	81.8	81.7	70.0	50.0	38.8	53.2	43.8	53.2
Co	12.5	16.0	14.1	14.2	14.6	14.5	16.4	15.8	10.1	18.9	15.6	16.1	11.3	9.8	10.8	11.7	11.1
Ni	31.7	38.7	37.0	35.1	37.0	35.3	38.0	36.8	22.6	42.8	37.5	40.2	25.4	22.7	25.5	27.4	28.0
Cu	28.7	33.4	34.6	29.8	30.9	34.4	32.9	35.5	17.6	44.0	42.3	48.6	21.3	18.1	15.6	31.4	25.8
Zn	92.3	68.4	82.1	61.8	67.8	62.5	68.6	61.1	41.8	82.1	122.5	63.7	49.0	33.7	51.2	37.8	44.7
Ga	14.3	19.6	20.4	18.4	18.4	16.9	18.0	15.3	12.4	19.9	21.5	16.6	12.5	9.2	12.2	10.7	13.6
Ge	1.1	1.3	1.3	1.2	1.3	1.3	1.5	1.3	1.4	1.5	1.8	1.3	1.0	0.7	1.0	0.8	0.9
Rb	92.1	129.7	132.4	117.4	118.1	112.1	119.2	103.5	80.8	135.4	137.1	111.8	80.4	62.2	82.2	70.0	90.7
Sr	421.8	237.3	283.6	271.5	603.4	497.3	244.4	328.3	302.8	292.2	248.1	758.1	1835.9	1497.2	1597.8	1867.4	398.8
Zr	140.2	150.2	164.6	160.8	120.3	133.6	148.4	142.2	187.2	140.1	149.5	128.6	117.7	92.2	141.9	92.4	91.0
Nb	11.6	13.7	14.3	13.4	11.8	12.0	13.3	11.5	11.4	13.6	14.4	11.7	10.2	6.3	7.9	7.6	7.5
Cs	8.4	11.6	11.3	10.4	10.3	10.0	10.5	8.7	5.6	12.8	12.4	10.5	6.4	5.3	7.1	6.0	8.0
Ba	326.0	438.3	474.5	403.6	410.3	436.9	423.0	416.5	341.5	461.6	480.1	439.8	704.5	389.7	519.8	592.6	347.3
Hf	3.7	4.0	4.3	4.2	3.2	3.6	4.0	3.8	4.8	3.8	4.0	3.5	3.2	2.4	3.7	2.4	2.4
Ta	0.9	1.0	1.1	1.0	0.9	0.9	1.0	0.8	0.8	1.0	1.1	0.9	0.8	0.5	0.6	0.6	0.6
Pb	26.4	19.8	25.7	18.1	24.7	24.8	19.5	32.0	14.7	40.6	16.3	50.4	17.0	27.8	15.1	38.9	18.5
Th	12.3	15.3	15.7	14.1	13.5	11.8	13.2	11.2	10.1	14.6	14.5	12.8	10.7	7.1	10.6	8.4	9.8
U	4.7	3.7	4.4	4.0	4.5	4.1	3.8	2.7	2.7	4.9	3.8	7.4	4.6	3.2	4.3	4.6	3.0
Sr/Ba	1.3	0.5	0.6	0.7	1.5	1.1	0.6	0.8	0.9	0.6	0.5	1.7	2.6	3.8	3.1	3.2	1.2
U_{auth}	2.9	1.5	2.1	1.9	2.5	2.1	1.7	0.8	1.1	2.5	1.4	5.4	3.1	2.1	2.9	3.3	1.4
U/Th	0.7	0.3	0.4	0.4	0.6	0.9	0.5	0.4	0.4	0.7	0.4	1.6	0.8	1.0	0.7	1.4	0.6

*Samples JS2-0111, JS2-0174, JS2-0505, JS2-0689 and JS2-0758 are endogenous fine-grained mixed sediments.

Table 3. TOC, REE contents and several associated parameters of fine-grained mixed sediments from the coring section (units in % and ppm)

Samples	Depth (m)	Y	La	Ce	Pr	Nd	Sm	Eu	Gd	Tb	Dy	Ho	Er	Tm	Yb	Lu	ΣREE	La _N /Yb _N	Samples	Depth (m)	TOC
JS2-0003	2001.0	28.2	33.8	71.0	8.6	31.5	5.9	1.2	5.5	0.8	4.8	1.0	2.8	0.4	2.8	0.4	170.6	1.18	T01	2008.9	0.32
JS2-0019	2006.1	26.0	32.3	67.7	8.2	29.9	5.6	1.1	5.1	0.8	4.5	0.9	2.6	0.4	2.6	0.4	162.0	1.19	T02	2019.4	0.32
JS2-0096	2029.1	26.9	32.2	67.9	8.1	29.9	5.6	1.2	5.3	0.8	4.6	0.9	2.7	0.4	2.7	0.4	162.6	1.17	T03	2029.9	0.37
JS2-0128	2040.1	26.7	32.3	67.5	8.1	30.2	5.7	1.1	5.3	0.8	4.7	0.9	2.7	0.4	2.7	0.4	162.8	1.17	T04	2041.8	0.23
JS2-0216	2069.0	26.2	30.3	64.0	7.6	28.1	5.4	1.1	5.0	0.7	4.4	0.9	2.6	0.4	2.6	0.4	153.5	1.14	T05	2059.3	0.28
JS2-0246	2079.7	26.1	30.7	64.2	7.7	28.3	5.4	1.1	5.0	0.7	4.5	0.9	2.7	0.4	2.7	0.4	154.6	1.10	T06	2073.0	0.38
JS2-0277	2089.4	22.1	24.1	50.5	6.4	23.7	4.6	1.0	4.5	0.6	3.8	0.7	2.1	0.3	2.0	0.3	124.7	1.15	T07	2092.9	0.36
JS2-0309	2099.1	27.5	32.1	68.2	8.2	30.0	5.7	1.2	5.3	0.8	4.7	0.9	2.7	0.4	2.7	0.4	163.3	1.17	T08	2111.7	0.31
JS2-0325	2103.9	22.6	26.6	55.2	6.6	24.3	4.6	0.9	4.4	0.6	3.9	0.8	2.2	0.3	2.2	0.3	133.0	1.18	T09	2121.0	0.26
JS2-0367	2119.1	28.4	33.8	71.0	8.6	31.6	6.0	1.2	5.5	0.8	4.9	1.0	2.9	0.4	2.8	0.4	170.8	1.15	T10	2136.3	0.31
JS2-0403	2128.9	24.7	30.3	63.3	7.6	27.7	5.2	1.0	4.9	0.7	4.2	0.9	2.5	0.4	2.4	0.4	151.4	1.22	T11	2155.4	0.33
JS2-0422	2133.8	26.4	31.3	65.7	7.9	29.1	5.5	1.1	5.2	0.8	4.6	0.9	2.6	0.4	2.6	0.4	158.0	1.17	T12	2166.2	0.33
JS2-0489	2153.5	25.4	29.5	61.8	7.4	27.6	5.3	1.1	5.0	0.7	4.2	0.8	2.4	0.4	2.3	0.3	149.0	1.22	T13	2175.5	0.22
JS2-0551	2173.4	25.8	30.3	62.2	7.5	27.6	5.3	1.1	5.0	0.7	4.3	0.9	2.5	0.4	2.4	0.4	150.6	1.21	T14	2182.1	0.34
JS2-0622	2192.4	27.9	33.5	69.8	8.3	30.8	5.8	1.2	5.4	0.8	4.7	1.0	2.8	0.4	2.7	0.4	167.6	1.19	T15	2190.4	0.31
JS2-0706	2217.6	24.0	28.6	59.1	7.1	26.1	4.9	1.0	4.7	0.7	4.0	0.8	2.4	0.4	2.3	0.3	142.4	1.20	T16	2198.5	0.29
JS2-0741	2227.7	28.9	34.4	72.5	8.7	32.1	6.1	1.2	5.6	0.8	4.9	1.0	2.9	0.4	2.9	0.4	174.0	1.17	T17	2208.7	0.21
JS2-0830	2252.7	24.3	28.1	58.9	7.1	26.0	5.0	1.0	4.7	0.7	4.2	0.8	2.4	0.4	2.3	0.3	142.0	1.16	T18	2223.8	0.30
JS2-0871	2262.8	29.0	34.7	73.5	8.8	32.5	6.3	1.2	5.8	0.8	5.0	1.0	2.8	0.4	2.8	0.4	176.2	1.21	T19	2232.0	0.62
JS2-0905	2272.9	29.6	34.5	74.0	8.8	32.6	6.3	1.2	5.8	0.8	5.1	1.0	2.9	0.4	2.9	0.4	176.9	1.15	T20	2242.8	0.35
JS2-0957	2287.3	27.6	33.0	69.5	8.3	30.5	5.8	1.2	5.4	0.8	4.7	0.9	2.7	0.4	2.7	0.4	166.2	1.21	T21	2263.2	0.52
JS2-0972	2292.4	24.6	29.4	61.8	7.4	27.1	5.1	1.0	4.8	0.7	4.2	0.8	2.4	0.4	2.4	0.4	147.9	1.19	T22	2280.0	0.25
JS2-1097	2327.2	24.0	27.7	56.4	6.4	25.5	4.8	1.0	4.6	0.7	4.1	0.8	2.3	0.4	2.3	0.4	137.3	1.17	T23	2286.4	0.42
JS2-1154	2342.5	26.7	32.1	66.2	7.5	29.7	5.6	1.2	5.3	0.8	4.7	0.9	2.6	0.4	2.5	0.4	159.9	1.23	T24	2302.1	0.36
JS2-1183	2352.6	25.7	32.6	68.3	7.8	30.9	5.9	1.2	5.6	0.8	4.7	0.9	2.5	0.4	2.4	0.4	164.5	1.32	T25	2307.3	0.66
JS2-1228	2367.5	26.7	33.1	65.9	7.3	28.8	5.4	1.1	5.3	0.8	4.6	0.9	2.5	0.4	2.4	0.4	158.8	1.36	T26	2329.4	0.41
JS2-1245	2372.6	25.3	31.7	64.0	7.2	28.2	5.3	1.1	4.9	0.7	4.4	0.9	2.5	0.4	2.5	0.4	154.2	1.23	T27	2338.9	0.49
JS2-1283	2387.5	26.3	31.8	64.7	7.4	28.8	5.5	1.1	5.0	0.8	4.7	0.9	2.6	0.4	2.6	0.4	156.7	1.19	T28	2349.9	0.30
JS2-1318	2397.4	23.0	26.9	55.5	6.2	24.7	4.7	1.0	4.4	0.7	4.0	0.8	2.3	0.3	2.3	0.4	134.3	1.13	T29	2362.9	1.11
JS2-0111*	2034.1	21.6	24.8	51.0	6.2	22.7	4.3	0.9	4.2	0.6	3.6	0.7	2.1	0.3	2.0	0.3	123.7	1.18	T30	2367.6	0.53
JS2-0174*	2054.1	16.1	18.2	36.7	4.1	16.0	3.0	0.6	3.0	0.4	2.6	0.5	1.5	0.2	1.5	0.2	88.6	1.20	T31	2383.5	0.38
JS2-0505*	2158.7	20.4	24.4	50.2	5.6	22.1	4.1	0.8	4.0	0.6	3.3	0.7	1.9	0.3	1.9	0.3	120.3	1.24	T32	2388.6	0.60
JS2-0689*	2212.7	17.2	21.0	42.9	4.9	19.1	3.6	0.7	3.5	0.5	2.9	0.6	1.7	0.2	1.6	0.2	103.4	1.25	T33	2390.2	0.42
JS2-0758*	2232.6	19.2	21.5	44.3	5.0	19.6	3.8	0.8	3.7	0.5	3.2	0.6	1.9	0.3	1.8	0.3	107.2	1.15	T34	2399.6	1.28

*Samples JS2-0111, JS2-0174, JS2-0505, JS2-0689 and JS2-0758 are endogenous fine-grained mixed sediments.

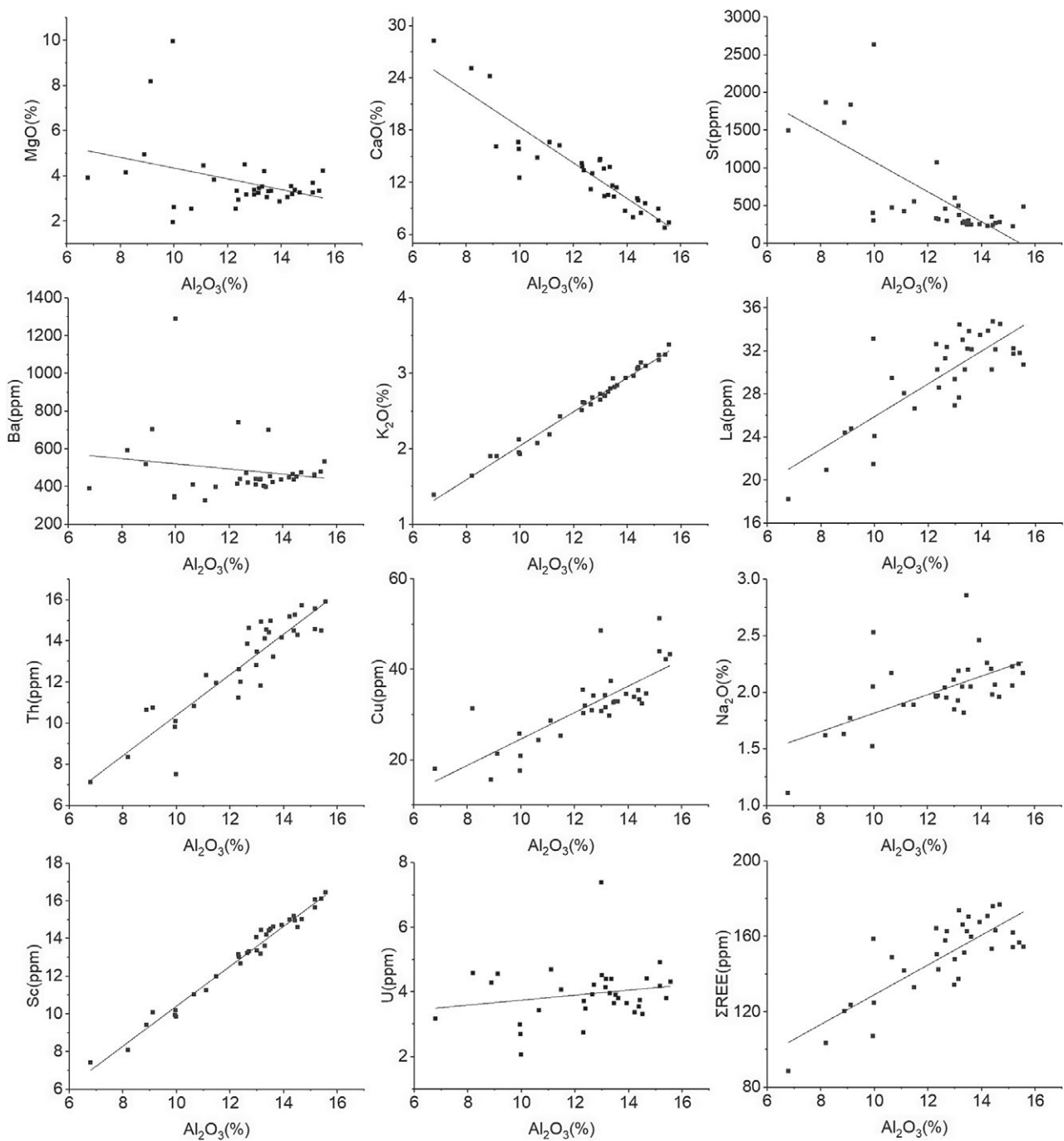


Fig. 6. Correlation of major, trace and rare earth elements of 34 samples of fine-grained mixed sediments from the coring section of the JS2 drillcore.

provenance during Middle Miocene time, making it excellent for reconstructing palaeoclimate (Fig. 1) (based on provenance analysis and seismic data). The chemical index of alteration (CIA) and Sr/Cu ratio can be used to quantify an evaluation of climate in contrast to Mg/Ca, FeO/MnO and $\text{Al}_2\text{O}_3/\text{MgO}$ (Sly, 1978; Nesbitt & Young, 1982). However, Cu is mainly supplied by detrital input under oxidizing conditions (Tribouillard *et al.* 2006), resulting in its unsuitability for reconstructing the climate. The aforementioned analysis indicated oxidizing conditions during the deposition of the mixed sediments, and the correlation analysis of the elements also showed characteristics of detrital input for Cu. Consequently, we only use authigenic Sr to reflect the climate changes here.

The CIA is defined as $\text{CIA} = (\text{Al}_2\text{O}_3 / (\text{Al}_2\text{O}_3 + \text{CaO}^* + \text{Na}_2\text{O} + \text{K}_2\text{O})) \times 100$, and all oxide contents are molar contents (Nesbitt & Young, 1982). CaO^* is the molar content of CaO in silicate minerals instead of in carbonate and phosphate (Young & Nesbitt, 1999). The calculation method of CaO^* content here is modelled after McLennan *et al.* (1993). Generally, low CIA values (50–60) reveal cold and arid climatic conditions with weak chemical weathering; moderate CIA values (60–80) reflect warm and humid climatic conditions with medium chemical weathering; and high CIA values (80–100) reveal hot and humid tropical climatic conditions with intensive chemical weathering (Nesbitt & Young, 1982; Fedo *et al.* 1995). The CIA values of the fine-grained mixed sediments

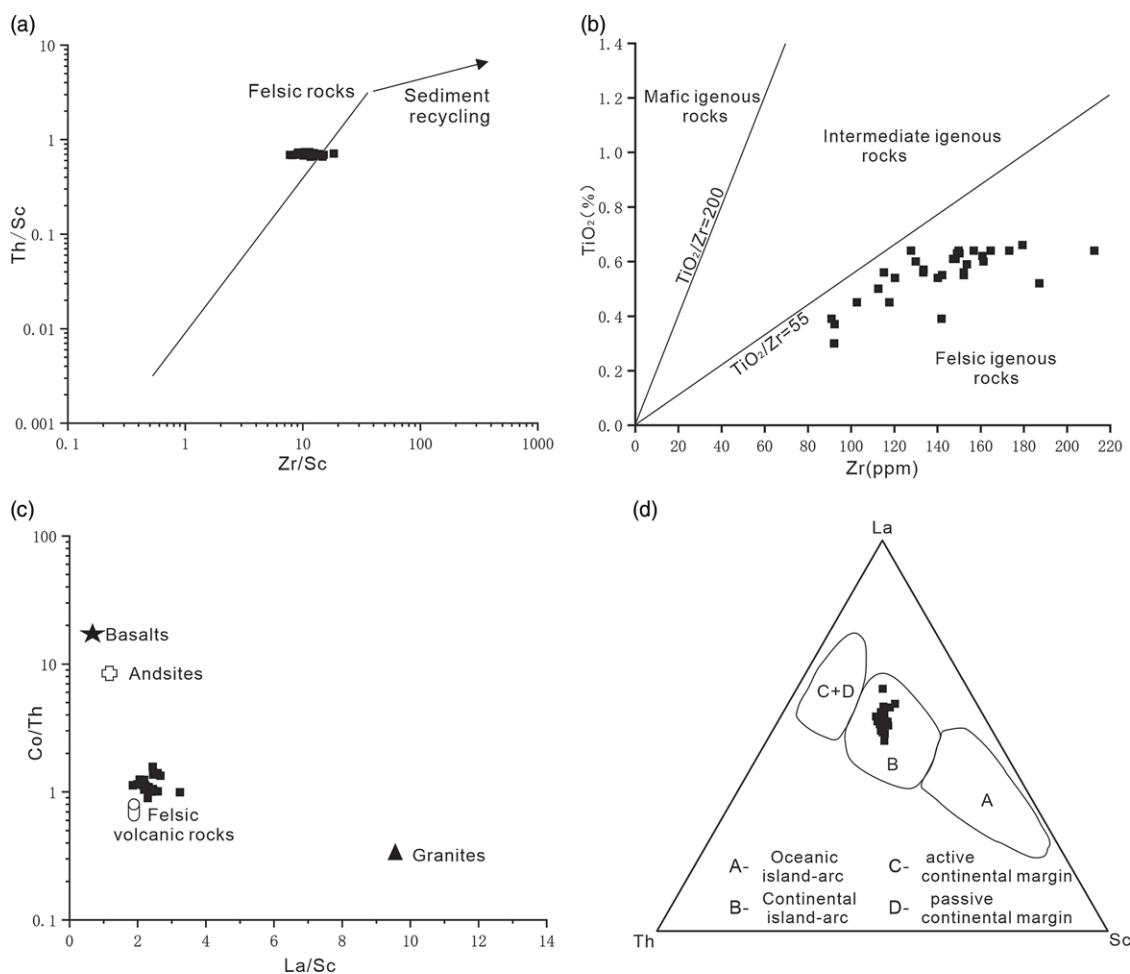


Fig. 7. Provenance identification plots for the fine-grained mixed sediments. (a) Th/Sc versus Zr/Sc. (b) TiO_2 versus Zr. (c) Co/Th versus La/Sc. (d) Ternary plot illustrating La, Th and Sc demonstrating the tectonic setting.

range from 49 to 60 in this study (Table 1), indicating cold and arid climatic conditions with weak chemical weathering (Fig. 9).

A large quantity of authigenic anhydrite and dolomite was deposited in this saline lake, indicating non-humid climatic conditions. However, interbedding of light-coloured sandy lamina and dark fine-grained lamina can be observed in the fine-grained mixed sediments; they are similar to typical seasonal lamina found in the Newark supergroup core, which was interpreted as a winter/summer growth pattern under a semi-arid climate (Olsen *et al.* 1996). This pattern is also reflected by the interbedding of light and dark laminations in stromatolites (de Wet *et al.* 2020), which are also observed in this study (Fig. 2b). In addition, the slump deposit in microstratification and a large number of climbing ripples observed in the mixed sediments also indicate a sedimentary environment controlled by a seasonal river (Shan *et al.* 2020) (Fig. 2c, d). Indeed, the Asian monsoon system was preliminarily established in Early Miocene time (Liu & Ding, 1998; Guo *et al.* 2002; Sun & Wang, 2005; Lin *et al.* 2015); subsequently, the retreats or expansions of the winter and summer monsoon mainly influenced precipitation in the Qaidam Basin (Miao *et al.* 2011). Therefore, we suggest the presence of a semi-arid climate in the Qaidam Basin during Middle Miocene time. Moreover, a strong seasonality dominated these climatic conditions, and the arid–humid fluctuation also contributed to the formation of fine-grained mixed sediments during this period.

The data also indicate a more arid tendency from sections B to A. There are higher values of the Sr/Ba ratio, Sr content and loss on ignition (LOI) in section A compared with section B; in particular, the endogenous fine-grained mixed sediments in section A have extremely high values (Fig. 9). As mentioned above, the higher values of the Sr/Ba ratio and Sr content indicate saline water conditions and a more arid climate (Wang & Wu, 1983; Zheng & Liu, 1999; Zhang *et al.* 2004). LOI refers to the percentage of the sample lost from the total mass under certain high-temperature conditions ($\sim 1000^\circ\text{C}$), which usually has a positive relationship with carbonate content and/or organic content in lacustrine sedimentary rocks (Bengtsson & Enell, 1986; Heiri *et al.* 2001). We note that the LOI values synergistically change with the Sr/Ba ratios and Sr values in the whole core section; specifically, the higher LOI values correspond with the lower TOC values in our study (Fig. 9). Thus, we conclude that the LOI values are mainly related to carbonate content here.

Together with the two conclusions drawn above, (1) the source of the fine-grained mixed sediments during Middle Miocene time is stable, both for the endogenous and exogenous fine-grained mixed sediments, and (2) the carbonate component in the mixed sediments studied here is mainly authigenic, we suggest that the higher LOI values do not affect the provenance, and they indicate a more arid climate. Furthermore, we interpret this phenomenon as indicating that relatively arid climatic conditions led to the

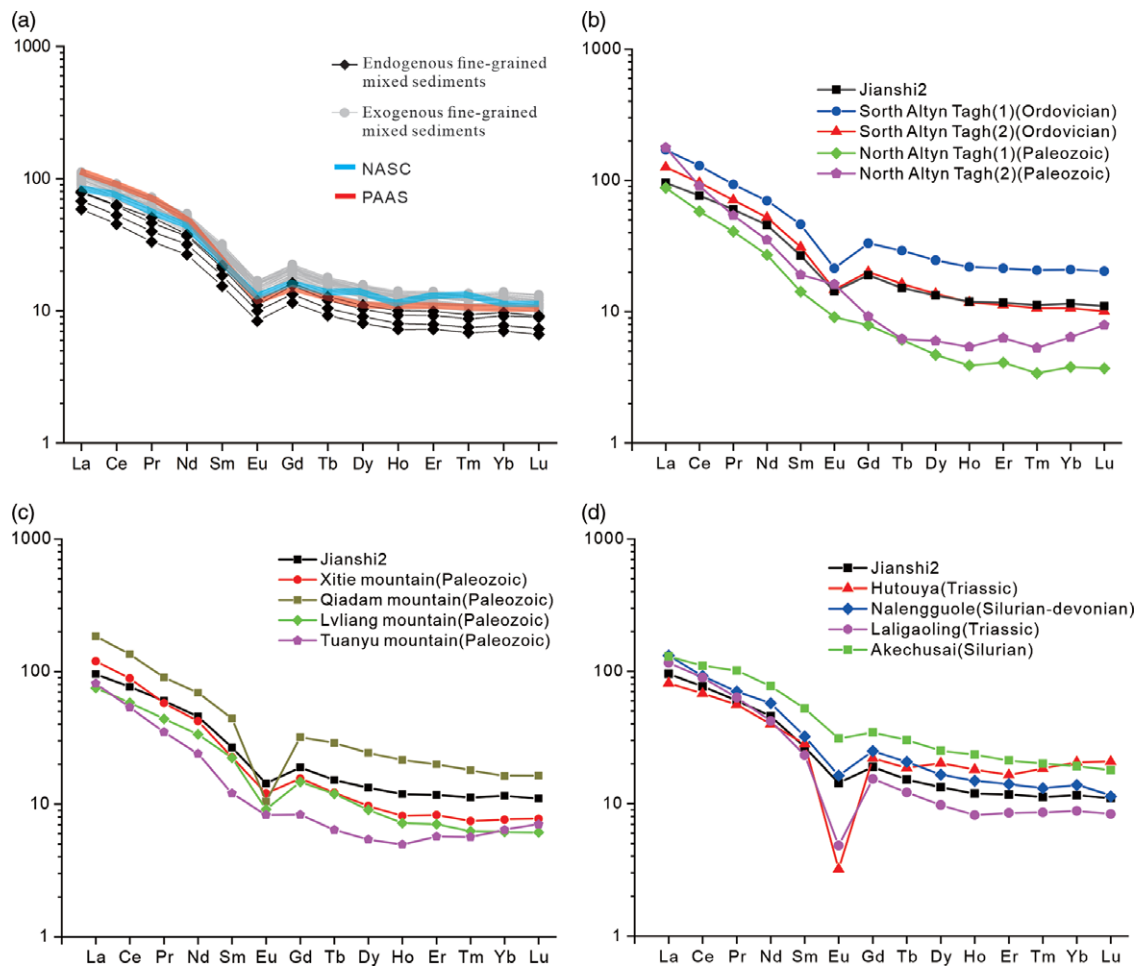


Fig. 8. (Colour online) (a) Chondrite-normalized pattern of rare earth elements of fine-grained mixed sediments, NASC and PAAS. (b) REE distribution pattern of granite in the north Altyn-Tagh and south Altyn-Tagh (Yang *et al.* 2012; Wu *et al.* 2014; Meng *et al.* 2016; Wu *et al.* 2017; Zheng *et al.* 2019). (c) REE distribution pattern of granite in the northern Qaidam Basin collected from Xitie Mountain, Qaidam Mountain, Lvliang Mountain and Tuanyu Mountain (Qin, 2012). (d) REE distribution pattern of granite in the East Kunlun Mountains collected from Hutouya, Nalengguole, Laligaoling and Aakechusai (1:250 000 regional geological survey report from Bukadaban Peak, Qinghai Geological Survey Institute, 2004; Wang *et al.* 2014; Hao *et al.* 2014; Li *et al.* 2015).

weakening of terrigenous clastic physical transportation and the enhancement of chemical precipitation.

The variation in TOC values of the fine-grained mixed sediments also indicates this climate change as occurring over time. The TOC values are lower than 0.4 % for all the samples from section A; meanwhile, more than half of the samples from section B have TOC values greater than 0.5 %, and some even greater than 1.0 % (Fig. 9; Table 3). More algal limestone interlayers were deposited in section B than in section A, indicating the prosperity of algae under a relatively humid climate and their contribution to the higher TOC.

In conclusion, the semi-arid climate dominates the salinity, carbonate contents and organic matter contents of the lacustrine basin in the Qaidam Basin during Middle Miocene time. Moreover, the multiple indexes indicate that a drying trend moved from section B to section A. However, the sedimentation rate and palaeoredox did not move with this climate change.

5.d. Palaeoclimate indicated by gamma-ray logging

Generally, gamma-ray values are consistently high in shale layers and low in carbonate layers (Gong & Li, 2020). Noticeably,

gamma-ray values represent the total effect of all radioactive elements (Th, K, U) in the stratum, and only Th and K contents usually have a linear relationship with shale contents (Chai *et al.* 2000; Wu *et al.* 2011). In our study, the gamma-ray values synergistically change with Th and K contents, indicating that the gamma-ray curves can be directly used for lithological characterization. The fine-grained mixed sediments studied here are homogeneous mixing products without obvious grain-size cycles, and they contain ~30 % (and even higher) authigenic carbonate; thus, their gamma-ray values better represent the mixing ratio of terrigenous clasts and intrabasinal carbonate. Consequently, the change in gamma-ray values is significant for reconstructing climatic evolution in saline lakes. The 2600 m long successive gamma-ray logging data from the whole JS2 drillhole show very good consistency with the $\delta^{18}\text{O}$ values spanning the past 20 million years from the ocean drilling core (Fig. 10c), indicating the effect of global climatic change on the Neogene palaeoclimate in the Qaidam Basin. Several climate change events can also be identified from this dataset (Fig. 10c), such as the MMCO, East Antarctic ice-sheet expansion, Asian monsoons intensification and West Antarctic ice-sheet expansion. In particular, the coring section of the JS2 drillhole overlapped with the MMCO event.

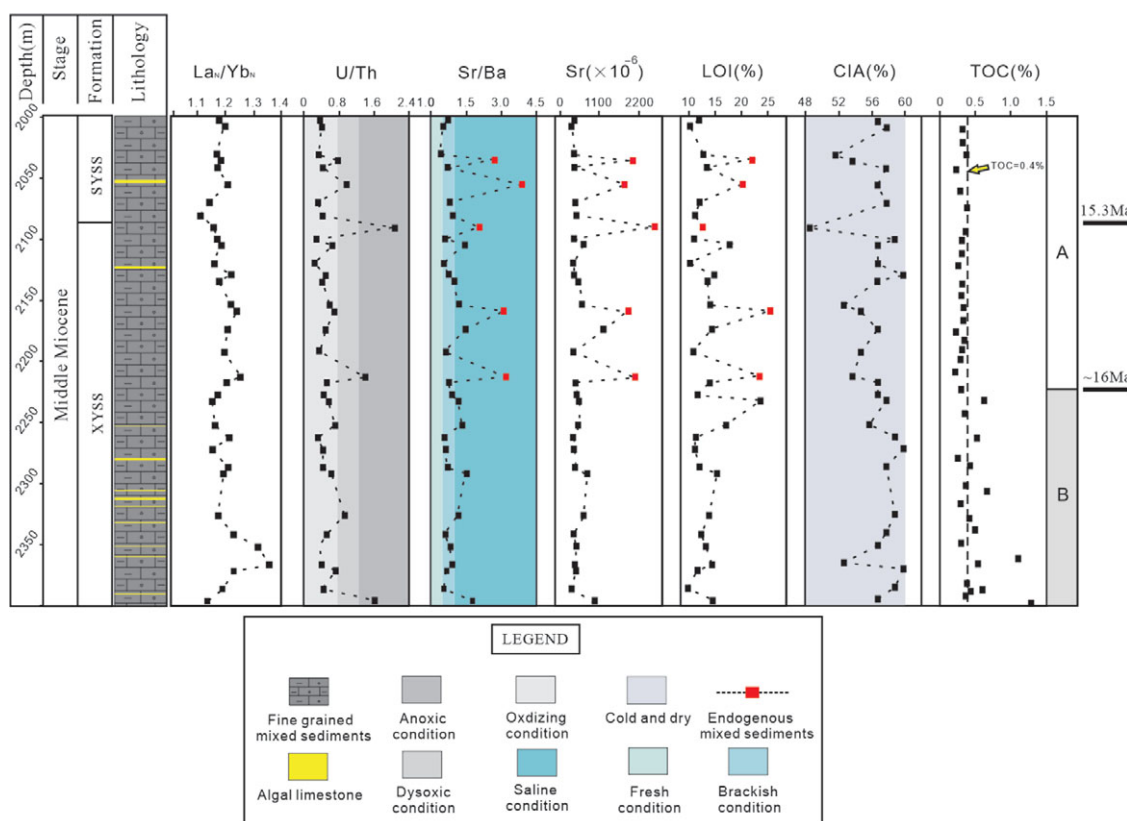


Fig. 9. (Colour online) Columns of indicators (U/Th, TOC, La_N/Yb_N , Sr/Ba, Sr, CIA, LOI) for fine-grained mixed sediments from the coring section.

6. Discussion

6.a. Age model of the JS2 drillcore

An accurate chronology is crucial for discussing the palaeoclimate within the Tibetan Plateau. Abundant work from the oilfield has established a basin-wide lithostratigraphic framework for the Qaidam Basin. According to this framework, the coring section of the JS2 drillhole studied here covers the bottom of the SYSS Fm and the top of the XYSS Fm. Therefore, the boundary age of the SYSS and XYSS fms was relatively easy to obtain for this study. However, the boundary age of the SYSS and XYSS fms in the Qaidam Basin remains controversial.

Based on palaeomagnetic age dating from some profiles in the basinal margins, two main models for the boundary age of the SYSS and XYSS fms suggest ages of ~13 Ma (Lu & Xiong, 2009; Chang *et al.* 2015) and 15.3 Ma (Fang *et al.* 2007; Wu *et al.* 2019; Fig. 10a). Notably, Wang *et al.* (2017) and Nie *et al.* (2019) hold the view that the boundary age of the SYSS and XYSS fms is 9.0 Ma, as estimated by the Honggou fauna, and the onset of basin filling occurred at ~25.5 Ma, challenging the previous interpretations. Therefore, we need to choose a boundary age for the SYSS and XYSS fms, as mentioned for this study.

We tend to prefer the estimate of 15.3 Ma after Fang *et al.* (2007) as the boundary age of the SYSS and XYSS fms here. This estimate is supported by the following facts. Many previous studies show that the climate changes of Central Asia were synchronous with global climate changes on a large scale during the Miocene Epoch. This is determined through a comparison of high-resolution proxy indexes, including pollen and magnetic susceptibility and oxygen isotopes from the Qaidam Basin, Tianshui Basin, Ningxia Basin, Linxia Basin, South China Sea and global sea (99-point moving

average; e.g. Zachos *et al.* 2001; Jiang & Ding, 2008; Tian *et al.* 2008; Hui *et al.* 2011; Miao *et al.* 2011; Guan *et al.* 2019; Figs 1a, 10b). Indeed, our gamma-ray data also support this view very well (Fig. 10b). By comparing this gamma-ray curve with global temperature and other climatic proxies, the MMCO event (17–15 Ma) can be easily identified, and the boundary of the SYSS and XYSS fms falls within this span and near the top of this event. Thus, the boundary age of the SYSS/XYSS fms is suggested to be ~15 Ma. Moreover, according to this method, the boundary age of the SYSS/SZG fms can be estimated as 8 Ma (Fig. 10c). In fact, the palaeomagnetic age of the boundary of the SYSS and SZG fms from different profiles in the Qaidam Basin is 8.1 Ma without obvious controversy (Zhang, 2006; Fang *et al.* 2007; Ji *et al.* 2017), further illustrating the reasonable approach of our age model (Fig. 10a).

According to this age model, the boundary age of sections A and B within the coring section is earlier than 15.3 Ma (Fig. 9). The above study shows that the sedimentary rate underwent no obvious change during the deposition of the coring section of the JS2 drillhole. Subsequently, given an assumption of a constant sedimentation rate, the boundary age of sections A and B is between 15.3 and 16 Ma. In any case, this boundary is within the MMCO event, meaning that there was a corresponding climatic change in the Qaidam Basin; this is reflected by the increase in carbonate-rich mixed sediments, decrease in algal limestone layers, decrease in lacustrine organic matter and the change in palaeosalinity in terms of basin filling.

6.b. Factors affecting climatic change during Middle Miocene time

Previous studies suggest that, during Middle Miocene time, there were warm and wet climatic conditions in monsoon-sensitive

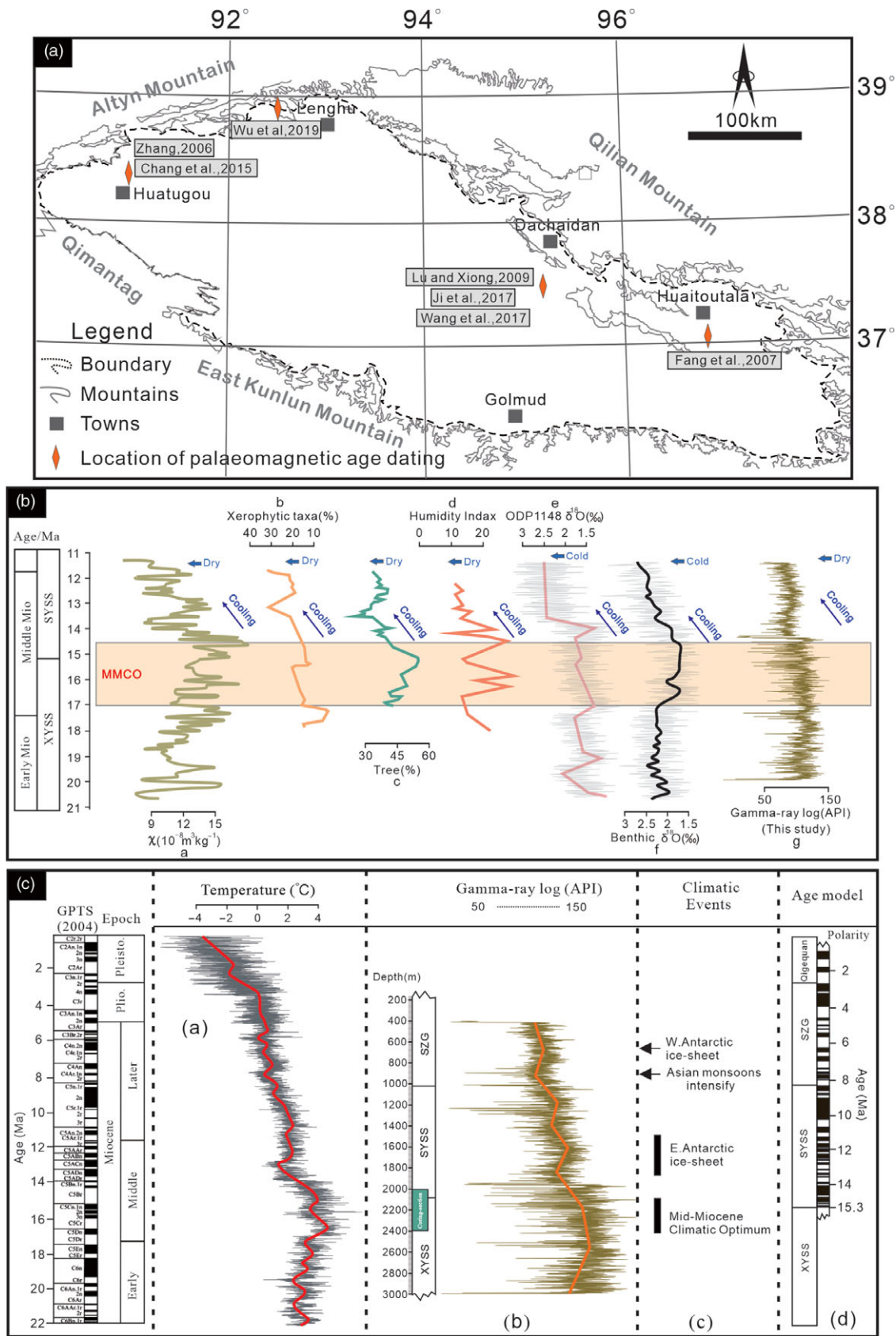


Fig. 10. (Colour online) (a) Palaeomagnetic age dating from some profiles in the basinal margin, which includes the boundary age of the SYSS/XYSS fms and the SYSS/SZG fms. (b) Comparison of regional and global climatic records during the Miocene Epoch, including the Middle Miocene Climatic Optimum and Middle Miocene Climate Cooling. a – magnetic susceptibility record of the HTG section in the Qaidam Basin (Guan et al. 2019); b – percentages of the pollen of xerophytic taxa from core KC-1 from the Qaidam Basin (Miao et al. 2011); c – tree pollen percentages from the Yanwan section in the Tianshui Basin (Hui et al. 2011); d – humidity index from the pollen record of the Sikouzi section (Jiang & Ding, 2008); e – $\delta^{18}\text{O}$ record of ODP Site 1148 (Tian et al. 2008); f – global marine $\delta^{18}\text{O}$ record (Zachos et al. 2001); g – the gamma-ray curves of the JS2 drillcore. (c) Age model of the JS2 drillcore. a – global temperature records (Westerhold et al. 2021); b – the JS2 drillcore gamma-ray log between 3000 and 400 m; c – climatic events during the Neogene Period (Zachos et al. 2001); d – age model in the Huaitoutala section (Fang et al. 2007).

regions, such as the Yunnan Basin (Lebreton-Anberrée *et al.* 2016), Loess Plateau (Dong *et al.* 2018), Tianshui Basin (Hou *et al.* 2014) and Xining Basin (Zan *et al.* 2015), and that the climate began drying at ~13 Ma. Taken together, these records indicate a relatively warm and humid climate during the MMCO period, and that the climate progressively deteriorated at 14–13 Ma in Central Asia, consistent with global climate changes. This climatic change in the Qaidam Basin can be illustrated by the successive gamma-ray logging data from the whole JS2 drillhole in this study; based on our age model, its onset time was ~14 Ma, which is related to the East Antarctic ice-sheet expansion (Fig. 10) and consistent with other research (Zachos *et al.* 2001; Westerhold *et al.* 2021). However, our geochemical data and analysis of petrology indicate that, during the MMCO period, the palaeoclimate in the Qaidam Basin was characterized as semi-arid; thus, we suggest that the palaeoclimate of the Qaidam Basin during the MMCO was dryer than once thought.

This suggestion is supported by other investigations; for example, the palynological analysis of the KC-1 core from the Qaidam Basin also shows that the climate became dryer throughout the Miocene Epoch (Miao *et al.* 2011, 2012). The existence of a dryer climate in the Qaidam Basin than in other areas in Central Asia during the MMCO period, as interpreted here, might be caused by the change of topography resulting from the uplift of the northeastern Tibetan Plateau at that time. Furthermore, numerous studies indicate that the main part of the Tibetan Plateau could have reached ~4 km or more as early as ~23 Ma, and then mainly affected the northeastern part against the background of a high-altitude plateau (e.g. Rowley & Currie, 2006; DeCelles *et al.* 2007; Rowley & Garzzone, 2007). The 'barrier effect' of the plateau may have altered the vapour transport pathways, preventing moisture from the south and southeast from moving into the Asian arid region and eventually creating the non-humid climate in the Qaidam Basin.

Notably, one climatic change that occurred earlier than 15 Ma identified in this study falls in the MMCO period. Indeed, this climatic fluctuation is seldom mentioned worldwide, and its cause is worthy of being discussed. The Paratethys that covered large areas of Central Asia during late Eocene–Oligocene times and influenced regional climate by immediately providing water vapour (Ramstein *et al.* 1997) had retreated from the Asian inland during Middle Miocene time (~15 Ma; Popova *et al.* 2004). The Early–Middle Miocene planktonic foraminifera at Miran River in the SE Tarim Basin, very close to the western Qaidam Basin, have not been observed in the post-Middle Miocene strata. Although attributing this planktonic foraminifer assemblage to either marine or terrestrial products remains open for discussion, the inference of a westward water retreat at that time seems reasonable (Ritts *et al.* 2008). Moreover, this palaeogeographic change coincided with the synchronous tectonic reorganization of the Altyn-Tagh fault system and northeastern Tibetan Plateau (Wu *et al.* 2019). Therefore, this tectonic and related palaeogeographic event may have created a barrier to water vapour in the Qaidam Basin from the west and consequently produced a drier climate in the Qaidam Basin.

Ultimately, global climate changes, as the primary factor, controlled the overall characteristics and changes of the Neogene climate in the Qaidam Basin, including the occurrence of the MMCO and the cooling and drying tendency. Regional events were the secondary factor contributing to the dryer climate in the Qaidam Basin relative to other areas in Central Asia and the secondary climatic change during the MMCO period.

7. Conclusion

Fine-grained mixed sediments, as a sensitive indicator of palaeoclimate, were widely deposited in the Miocene Qaidam Lake. These rocks were formed by the mixing of siliciclastic, carbonate and clay components, and the relative content of each is less than 50%. The long-term global cooling trend and typical abrupt events (such as the MMCO during 17–15 Ma) in the past 20 million years are well identified in the Qaidam Basin via petrological observation, geochemical data and 2600 m long successive gamma-ray logging data analysis of the fine-grained mixed sediments. The difference, however, is that the Middle Miocene Qaidam lacustrine basin developed in oxidizing, high-sedimentation rate and brackish-saline water conditions in a semi-arid climate, indicating a dryer climate in the Qaidam Basin than in the monsoon-sensitive regions of Central Asia during the MMCO period. Also identified in this study is one climatic change that occurred before 15 Ma; this is characterized by an increase in carbonate-rich mixed sediments, a decrease in algal limestone layers, a decrease in lacustrine organic matter and a change in palaeosalinity in terms of basin filling. This event falls in the MMCO period and is seldom mentioned worldwide; we interpret it as the potential result of regional tectonic events, such as the retreat of the Paratethys from Central Asia at ~15 Ma and the synchronous tectonic reorganization of the Altyn-Tagh fault system and the northeastern Tibetan Plateau.

We suggest that global climate changes were the primary factor affecting the Neogene climate in the Qaidam Basin, influencing the overall climatic characteristics and cooling tendency; meanwhile, regional events were secondary, resulting in the dryer climate in the Qaidam Basin relative to other areas in Central Asia during the MMCO period, and the secondary climatic change during the MMCO period.

Acknowledgements. This study was funded by grants from the National Natural Science Foundation of China (#41602111). We thank the Exploratory Development Institute of Qinghai Oilfield Company for providing part of the data used in this analysis. We thank Professor Lin Xiubin and other anonymous reviewers for their valuable reviews of earlier versions of this manuscript.

References

- Bengtsson L and Enell M (1986) Chemical analysis. In *Handbook of Holocene Palaeoecology and Palaeohydrology* (ed. BE Berglund), pp. 423–51. Chichester: John Wiley & Sons Ltd.
- Böhme M (2003) The Miocene Climatic Optimum: evidence from ectothermic vertebrates of Central Europe. *Palaeogeography, Palaeoclimatology, Palaeoecology* **195**, 389–401.
- Böning P, Brumsack HJ, Böttcher ME, Schnetger B, Kriete C, Kallmeyer J and Borchers SL (2004) Geochemistry of Peruvian near-surface sediments. *Geochimica et Cosmochimica Acta* **68**, 4429–51.
- Brooks GR, Doyle LJ, Suthard BC, Locker SD and Hine AC (2003) Facies architecture of the mixed carbonate/siliciclastic inner continental shelf of west-central Florida: implications for Holocene barrier development. *Marine Geology* **200**, 325–49.
- Campbell AE (2005) Shelf-geometry response to changes in relative sea level on a mixed carbonate-siliciclastic shelf in the Guyana Basin. *Sedimentary Geology* **175**, 259–75.
- Chai XY, Li LR and Liu ZY (2000) Application of natural gamma ray spectrometry log data in Zhangdong area. *Well Logging Technology* **24**, 118–24 (in Chinese)
- Chang H, Li L, Qiang X, Garzzone CN, Pullen A and An Z (2015) Magnetostratigraphy of Cenozoic deposits in the western Qaidam Basin

- and its implication for the surface uplift of the northeastern margin of the Tibetan Plateau. *Earth and Planetary Science Letters* **430**, 271–83.
- Chiarella D, Longhitano SG and Tropeano M** (2017) Types of mixing and heterogeneities in siliciclastic-carbonate sediments. *Marine and Petroleum Geology* **88**, 617–27.
- Cowgill E, Yin A, Arrowsmith JR, Feng WX and Shuanhong Z** (2004) The Akato Tagh bend along the Altyn Tagh fault, NW Tibet 1. Cenozoic structure, smoothing by vertical-axis rotation, and the effect of topographic stresses on borderland faulting. *Geological Society of America Bulletin* **116**, 1423–42.
- de Wet CB, de Wet AP, Linda G, Driscoll E, Patzkowsky S, Xu C,igliotti S and Feitl M** (2020) Pliocene short-term climate changes preserved in continental shallow lacustrine-palustrine carbonates: Western Opache Formation, Atacama Desert, Chile. *Geological Society of America Bulletin* **132**, 1795–816.
- DeCelles PG, Quade J, Kapp P, Fan MJ, Dettman DL and Ding L** (2007) High and dry in Central Tibet during the Late Oligocene. *Earth and Planetary Science Letters* **253**, 389–401.
- Dettman D, Fang XM, Garzzone C and Li JJ** (2003) Uplift-driven climate change at 12 Ma: a long $\delta^{18}\text{O}$ record from the NE margin of the Tibetan plateau. *Earth and Planetary Science Letters* **214**, 267–77.
- Dong JB, Liu ZH, An ZS, Liu WG, Zhou WJ, Qiang XK and Lu FY** (2018) Mid Miocene C_4 expansion on the Chinese Loess Plateau under an enhanced Asian summer monsoon. *Journal of Asian Earth Sciences* **158**, 153–9.
- Fang XM, Zhang WL, Meng QQ, Gao JP, Wang XM, King J, Song CH, Dai S and Miao YF** (2007) High-resolution magnetostratigraphy of the Neogene Huaitoutala section in the eastern Qaidam Basin on the NE Tibetan Plateau, Qinghai Province, China and its implication on tectonic uplift of the NE Tibetan Plateau. *Earth and Planetary Science Letters* **258**, 293–306.
- Fedo CM, Nesbitt HW and Young GM** (1995) Unraveling the effects of K-metasomatism in sedimentary rocks and paleosols with implications for palaeoweathering conditions and provenance. *Geology* **23**, 921–4.
- Flower BP and Kennett JP** (1994) The middle Miocene climatic transition – East Antarctic ice-sheet development, deep-ocean circulation and global carbon cycling. *Palaeogeography, Palaeoclimatology, Palaeoecology* **108**, 537–55.
- Fu XG, Wang J, Chen WB, Feng XL, Wang D, Song CY and Zeng SQ** (2015) Organic accumulation in lacustrine rift basin: constraints from mineralogical and multiple geochemical proxies. *International Journal of Earth Sciences* **104**, 495–511 (in Chinese).
- Garcia-Garcia F, Soria JM, Viseras C and Fernandez J** (2009) High frequency rhythmicity in a mixed siliciclastic-carbonate shelf (Late Miocene, Guadix basin, Spain): a model of interplay between climatic oscillations, subsidence, and sediment dispersal. *Journal of Sedimentary Research* **79**, 302–15.
- Gold RD, Cowgill E, Arrowsmith JR, Chen X, Sharp WD, Cooper KM and Wang XF** (2011) Faulted terrace risers place new constraints on the late Quaternary slip rate for the central Altyn Tagh fault, northwest Tibet. *Geological Society of America Bulletin* **123**, 958–78.
- Gong Z and Li M** (2020) Astrochronology of the Ediacaran Shuram carbon isotope excursion, Oman. *Earth and Planetary Sciences Letters* **547**, 116462. doi: [10.1016/j.epsl.2020.116462](https://doi.org/10.1016/j.epsl.2020.116462).
- Gromet LP, Haskin LA, Korotev RF and Dymek RF** (1985) The “North American shale composite”: its compilation, major and trace element characteristics. *Geochimica et Cosmochimica Acta* **48**, 2469–82.
- Guan C, Chang H, Yan M, Li LY, Xia MM, Zan JB and Liu SC** (2019) Rock magnetic constraints for the Mid-Miocene Climatic Optimum from a high-resolution sedimentary sequence of the northwestern Qaidam Basin, NE Tibetan Plateau. *Palaeogeography, Palaeoclimatology, Palaeoecology* **532**, 109263. doi: [10.1016/j.palaeo.2019.109263](https://doi.org/10.1016/j.palaeo.2019.109263).
- Guo ZT, Ruddiman WF, Hao QZ, Wu HB, Qiao YS, Zhu RX, Peng SZ, Wei JJ, Yuan BY and Liu TS** (2002) Onset of Asian desertification by 22 Myr ago inferred from loess deposits in China. *Nature* **416**, 159–63.
- Guo ZQ, Wang ZL, Li XF, Zhang L, Zhang SS and Kong Y** (2009) Preliminary study on sedimentary facies of the Neogene in Yiliping area, Qaidam Basin. *Journal of Palaeogeography* **11**, 284–92 (in Chinese).
- Hao NN, Yuan WM, Zhang AK, Cao JH, Chen XN, Feng YL and Li X** (2014) Late Silurian to Early Devonian granitoids in the Qimantage area, East Kunlun Mountains: LA-ICP-MS zircon U–Pb ages, geochemical features and geological setting. *Geological Review* **60**, 201–15.
- Hatch JR and Leventhal JS** (1992) Relationship between inferred redox potential of the depositional environment and geochemistry of the Upper Pennsylvanian (Missourian) Stark Shale Member of the Dennis Limestone, Wabunsee County, Kansas, U.S.A. *Chemical Geology* **99**, 65–82.
- Hayashi KI, Fujisawa H, Holland HD and Ohmoto H** (1997) Geochemistry of ca. 1.9 Ga sedimentary rocks from northeastern Labrador, Canada. *Geochimica et Cosmochimica Acta* **61**, 4115–37.
- Heiri O, Lotter AF and Lemcke G** (2001) Loss on ignition as a method for estimating organic and carbonate content in sediments: reproducibility and comparability of results. *Journal of Paleolimnology* **25**, 101–10.
- Holbourn A, Kuhnt W, Lyle M, Schneider L, Romero O and Anderson N** (2014) Middle Miocene climate cooling linked to intensification of eastern equatorial Pacific upwelling. *Geology* **42**, 19–22.
- Hou ZF, Li JJ, Song CH, Zhang J, Hui ZC, Chen SY and Xian F** (2014) Understanding Miocene climate evolution in northeastern Tibet: stable carbon and oxygen isotope records from the Western Tianshui Basin. *Journal of Earth Science* **25**, 357–65.
- Huang C and Hinnov L** (2014) Evolution of an Eocene–Oligocene saline lake depositional system and its controlling factors, Jiangnan basin, China. *Journal of Earth Science* **25**, 959–76.
- Huang C and Hinnov L** (2019) Astronomically forced climate evolution in a saline lake record of the middle Eocene to Oligocene, Jiangnan Basin, China. *Earth and Planetary Science Letters* **528**, 115846. doi: [10.1016/j.epsl.2019.115846](https://doi.org/10.1016/j.epsl.2019.115846).
- Hui ZC, Li JJ, Xu QH, Song CH, Zhang J, Wu FL and Zhao ZJ** (2011) Miocene vegetation and climatic changes reconstructed from a sporopollen record of the Tianshui Basin, NE Tibetan Plateau. *Palaeogeography, Palaeoclimatology, Palaeoecology* **308**, 373–82.
- Hui ZC, Zhang J, Ma ZH, Li XM, Peng TJ, Li JJ and Wang B** (2018) Global warming and rainfall: lessons from an analysis of Mid-Miocene climate data. *Palaeogeography, Palaeoclimatology, Palaeoecology* **512**, 106–17.
- Ji J, Zhang K, Clift PD, Zhuang G, Song B, Ke X and Xu Y** (2017) High-resolution magnetostratigraphic study of the Paleogene–Neogene strata in the Northern Qaidam Basin: implications for the growth of the Northeastern Tibetan Plateau. *Gondwana Research* **46**, 141–55.
- Jiang HC and Ding ZL** (2008) A 20 Ma pollen record of East-Asian summer monsoon evolution from Guyuan, Ningxia, China. *Palaeogeography, Palaeoclimatology, Palaeoecology* **265**, 30–8.
- Jiang ZX, Liang C and Wu J** (2013) Several issues in sedimentological studies on hydrocarbon-bearing fine-grained sedimentary rocks. *Acta Petrolei Sinica* **34**, 1031–9 (in Chinese).
- Jones B, David AC and Manning B** (1994) Comparison of geochemical indices used for the interpretation of palaeoredox conditions in ancient mudstones. *Chemical Geology* **111**, 111–29.
- Lebreton-Anberrée J, Li SH, Li SF, Spicer RA, Zhang ST, Su T, Deng CL and Zhou ZK** (2016) Lake geochemistry reveals marked environmental change in Southwest China during the Mid Miocene Climatic Optimum. *Science Bulletin* **61**, 897–910.
- Li K, Gao YB, Qian B, He SY, Liu YL, Zhang ZW, Zhang JW and Wang YL** (2015) Geochronology, geochemical characteristics and Hf isotopic compositions of granite in the Hutouya deposit, Qimantag, East Kunlun. *Geology in China* **42**, 630–45 (in Chinese).
- Lin XB, Wyrwoll KH, Chen H and Cheng X** (2015) On the timing and forcing mechanism of a mid-Miocene arid climate transition at the NE margins of the Tibetan Plateau: stratigraphic and sedimentologic evidence from the Sikouzi section. *International Journal of Earth Sciences* **105**, 1–11.
- Liu TS and Ding ZL** (1998) Chinese loess and the paleomonsoon. *Annual Review of Earth and Planetary Sciences* **26**, 111–45.
- Lu HJ and Xiong SF** (2009) Magnetostratigraphy of the Dahonggou section, northern Qaidam Basin and its bearing on Cenozoic tectonic evolution of the Qilian Shan and Altyn Tagh fault. *Earth and Planetary Science Letters* **288**, 539–50.
- McLennan SM, Hemming S, McDaniell DK and Hanson GN** (1993) Geochemical approaches to sedimentation, provenance, and tectonics. *Geological Society of America Bulletin* **285**, 21–40.

- Meng LT, Chen BL, Wang Y, Sun Y, Wu Yu, Zhang WG and He JT (2016) Timing of Early Paleozoic tectonic regime transition in north Altun: evidence from granite. *Geotectonica et Metallogenia* **040**, 295–307 (in Chinese).
- Miao YF, Fang XM, Herrmann M, Wu FL, Zhang YZ and Liu DL (2011) Miocene pollen record of KC-1 core in the Qaidam Basin, NE Tibetan Plateau and implications for evolution of the East Asian monsoon. *Palaeogeography, Palaeoclimatology, Palaeoecology* **299**, 30–8.
- Miao YF, Herrmann M, Wu FL, Yan XL and Yang SL (2012) What controlled Mid–Late Miocene long-term aridification in Central Asia? – global cooling or Tibetan Plateau uplift: a review. *Earth Science Reviews* **112**, 155–72.
- Moradi AV, Sari A and Akkaya P (2016) Geochemistry of the Miocene oil shale (Hançili Formation) in the Çankırı Çorum Basin, Central Turkey: implications for paleoclimate conditions, source area weathering, provenance and tectonic setting. *Sedimentary Geology* **341**, 289–303.
- Mount JF (1984) Mixing of siliciclastic and carbonate sediments in shallow shelf environments. *Geology* **12**, 432–5.
- Nesbitt HW and Young GM (1982) Early Proterozoic climates and plate motions inferred from major element chemistry of lutites. *Nature* **299**, 715–7.
- Nie J, Ren X, Saylor JE, Su Q, Horton BK, Bush MA, Chen W and Pfaff K (2019) Magnetic polarity stratigraphy, provenance, and paleoclimate analysis of Cenozoic strata in the Qaidam basin, NE Tibetan Plateau. *Geological Society of America Bulletin* **132**, 310–20.
- Olsen PE, Watkins AJ, Boei JJ, Vermeulen S, Natarajan AT and Kent DV (1996) Milankovitch climate forcing in the tropics of Pangaea during the Late Triassic. *Palaeogeography, Palaeoclimatology, Palaeoecology* **122**, 1–26.
- Popova SV, Rögl F, Rozanov AY, Steininger FF, Scherba IG and Kovac M (eds) (2004) Lithological-paleogeographic maps of Paratethys: 10 maps Late Eocene to Pliocene. *Courier Forschungsinstitut Senckenberg* **250**, 1–46.
- Qin HP (2012) *Petrology of early Paleozoic granites and their relation to tectonic evolution of orogen in the North Qinlian Orogenic Belt*. Ph.D. thesis, Chinese Academy of Geological Sciences, Beijing, China. Published thesis (in Chinese).
- Qinghai Geological Survey Institute (2004) *J46C004001 (Bukadaban Peak) 1:250000*. Regional Geological Survey Report.
- Ramstein G, Fluteau F and Besse J (1997) Effect of orogeny: plate motion and land-sea distribution on Eurasian climate change over the past 30 million years. *Nature* **386**, 788–95.
- Reitz A, Pfeifer K, Lange GJ and Klump J (2004) Biogenic barium and the detrital Ba/Al ratio: a comparison of their direct and indirect determination. *Marine Geology* **204**, 289–300.
- Retallack GJ (1992) Middle Miocene fossil plants from Fort Ternan (Kenya) and evolution of African grasslands. *Paleobiology* **18**, 383–400.
- Rieser AB, Neubauer F, Liu Y and Ge X (2005) Sandstone provenance of north-western sectors of the intracontinental Cenozoic Qaidam basin, western China: tectonic vs. climatic control. *Sedimentary Geology* **177**, 1–18.
- Ritts BD, Yue Y, Graham SA, Sobel ER, Abbink OA and Stockli D (2008) From sea level to high elevation in 15 million years: uplift history of the northern Tibetan plateau margin in the Altun Shan. *American Journal of Science* **308**, 657–78.
- Roussiez V, Ludwig W, Probst JL and Monaco A (2005) Background levels of heavy metals in surficial sediments of the gulf of lions (NW Mediterranean): an approach based on ¹³³Cs normalization and lead isotope measurements. *Environmental Pollution* **138**, 167–77.
- Rowley DB and Currie BS (2006) Palaeo-altimetry of the late Eocene to Miocene Lunpola basin, central Tibet. *Nature* **439**, 677–81.
- Rowley DB and Garzone CN (2007) Stable isotope-based paleoaltimetry. *Annual Review of Earth and Planetary Sciences* **35**, 463–508.
- Savin SM, Douglas RG and Stehli FG (1975) Tertiary marine paleotemperatures. *Geological Society of America* **86**, 1499–510.
- Sha QA (2001) Discussion on mixing deposit and Hunji rock. *Journal of Palaeogeography* **3**, 63–6 (in Chinese).
- Shan X, Shi X, Clift PD, Seddique AA, Liu S, Tan C, Liu J, Hasan R, Li J and Song Z (2020) Sedimentology of the modern seasonal lower Ganges river with low inter-annual peak discharge variance, Bangladesh. *Journal of the Geological Society, London* **178**. doi: [10.1144/jgs2020-094](https://doi.org/10.1144/jgs2020-094).
- Shields G and Stille P (2001) Diagenetic constraints on the use of cerium anomalies as paleoseawater redox proxies: an isotopic and REE study of Cambrian phosphorites. *Chemical Geology* **175**, 29–48.
- Sly PG (1978) Sedimentary processes in lakes. In *Lakes: Chemistry, Geology, Physics* (ed. A Lerman), pp. 79–83. Berlin: Springer-Verlag.
- Song YG, Wang QS, An ZS, Qiang XK, Dong JB, Chang H, Zhang MS and Guo XH (2017) Mid-Miocene Climatic Optimum: clay mineral evidence from the red clay succession, Longzhong Basin, Northern China. *Palaeogeography, Palaeoclimatology, Palaeoecology* **512**, 46–55.
- Sun XJ and Wang PX (2005) How old is the Asian monsoon system? Palaeobotanical records from China. *Palaeogeography, Palaeoclimatology, Palaeoecology* **222**, 181–222.
- Sun ZM, Yang ZY, Ge XH, Pei JL, Guo XZ, Li WM, Ma ZQ and Xu SJ (2004) Advances in the study of the Paleogene magnetostratigraphy on the northwestern margin of the Qaidam Basin. *Geological Bulletin of China* **23**, 899–902 (in Chinese).
- Tapponnier P (2001) Oblique stepwise rise and growth of the Tibet Plateau. *Science* **294**, 1671–7.
- Taylor SR and McLennan SM (1985) The continental crust: its composition and evolution. *The Journal of Geology* **94**, 57–72.
- Tenger T, Liu WH, Xu YC, Chen JF, Hu K and Gao CL (2006) Comprehensive geochemical identification of highly evolved marine hydrocarbon source rocks: organic matter, palaeo-environment and development of effective hydrocarbon source rocks. *Chinese Journal of Geochemistry* **25**, 333–40.
- Tian J, Zhao QH, Wang PX, Li QY and Cheng XR (2008) Astronomically modulated Neogene sediment records from the South China Sea. *Palaeoceanography* **23**, 3210. doi: [10.1029/2007PA001552](https://doi.org/10.1029/2007PA001552).
- Tribouillard N, Algeo TJ, Lyons T and Riboulleau A (2006) Trace metals as paleoredox and paleoproductivity proxies: an update. *Chemical Geology* **232**, 12–32.
- Tribouillard N, Desprairies A, Lallier-Vergès E, Moureau N, Ramdani A and Ramanampisoa L (1994) Geochemical study of organic-rich cycles from the Kimmeridge Clay Formation of Yorkshire (G.B.): productivity vs. anoxia. *Palaeogeography, Palaeoclimatology, Palaeoecology* **108**, 165–81.
- Wang BZ, Chen J, Luo ZH, Chen FB, Wang T and Guo GE (2014) Spatial and temporal distribution of Late Permian Early Jurassic intrusion assemblages in eastern Qimantag, East Kunlun, and their tectonic settings. *Acta Petrologica Sinica* **30**, 3213–28.
- Wang AH, Wang ZH, Liu JK, Xu NC and Li HL (2021) The Sr/Ba ratio response to salinity in clastic sediments of the Yangtze River Delta. *Chemical Geology* **559**, 119923. doi: [10.1016/j.chemgeo.2020.119923](https://doi.org/10.1016/j.chemgeo.2020.119923).
- Wang YY and Wu P (1983) Geochemical criteria of sediments in the coastal area of Jiangsu and Zhejiang Provinces. *Journal of Tongji University* **11**, 82–90 (in Chinese).
- Wang WT, Zheng WJ, Zhang PZ, Li Q, Kirby E, Yuan DY, Zheng DW, Liu CC, Wang ZC, Zhang HP and Pang JZ (2017) Expansion of the Tibetan Plateau during the Neogene. *Nature Communications* **8**, 15887. doi: [10.1038/ncomms15887](https://doi.org/10.1038/ncomms15887).
- Webb SD (1997) A history of savanna vertebrates in the New World. Part I: North America. *Annual Review of Ecology Systematics* **8**, 355–80.
- Westerhold T, Marwan N, Drury AJ, Liebrand D, Agnini C and Anagnostou E (2021) An astronomically dated record of Earth's climate and its predictability over the last 66 million years. *Science* **369**, 1383–7.
- Wu Y, Chen ZL, Chen BL, Wang Y, Meng LT, He JT, Wang B and Han MM (2017) Geochemistry, zircon SHRIMP U–Pb dating and Hf isotopic compositions of the monzogranite from the southern Kaladawan of North Altun and their implications for crust-mantle interaction. *Acta Geologica Sinica* **91**, 1227–44 (in Chinese).
- Wu CL, Gao YH, Lei M, Qin HP, Liu CH, Li MZ, Frost BR and Wooden JL (2014) Zircon SHRIMP U–Pb dating, Lu–Hf isotopic characteristics and petrogenesis of the Palaeozoic granites in Mangya area, southern Altun, NW China. *Acta Petrologica Sinica* **30**, 2297–23 (in Chinese).
- Wu XS, Guo JJ, Huang YJ and Fu JW (2011) Well logging proxy of the Late Cretaceous Palaeoclimate change in Songliao Basin. *Journal of Palaeogeography* **13**, 103–10 (in Chinese).
- Wu J, Jiang ZX, Pan YB, Zhang Q and He LQ (2016) Lacustrine fine-grained depositional model: a case study of the upper submember of the fourth

- Member of Paleogene Shahejie Formation in Dongying sag. *Acta Petrologica Sinica* 37, 1080–9 (in Chinese).
- Wu L, Lin XB, Cowgill E, Xiao AC, Cheng XG, Chen HL, Zhao HF, Shen Y and Yang SF** (2019) Middle Miocene reorganization of the Altyn Tagh fault system, Northern Tibetan plateau. *Geological Society of America Bulletin* 131, 1157–78.
- Xiong Y, Wu KY, Tan XC, Zhang YS, Bo Y, Ling R, Ling L, Yun L, Qiao YP, and Wang XF** (2018) Influence of lake-level fluctuation on the mixed saline lacustrine carbonate reservoir: a case study. *Journal of Paleogeography* 20, 855–68 (in Chinese).
- Xu W, Chen KY, Cao ZL, Xue JQ, Xiao P and Wang WT** (2014) Original mechanism of mixed sediments in the saline lacustrine basin. *Acta Petrologica Sinica* 30, 1804–16 (in Chinese).
- Xu W, Du XF, Huang XB, Song ZQ and Li ZY** (2018) Research advances and critical issues of “mixed siliciclastic and carbonate sediments”. *Acta Sedimentologica Sinica* 37, 225–38 (in Chinese).
- Xu ZQ, Yang JS, Li HB, Zhang JX, Zeng LC and Jiang M** (2006) The Qinghai-Tibet Plateau and continental dynamics: a review on terrain tectonics, collisional orogenesis, and processes and mechanisms for rise of Plateau. *Geology in China* 33, 221–38 (in Chinese).
- Yan JH, Pu XG, Zhou LH, Chen S and Han W** (2015) Naming method of fine-grained sedimentary rocks on basis of X-ray diffraction data. *China Petroleum Exploration* 20, 48–54 (in Chinese).
- Yang WQ, Liu L, Ding HB, Xiao PX, Cao YT and Kang L** (2012) Geochemistry, geochronology and zircon Hf isotopes of the Dimunalike granite in South Altyn Tagn and its geological significance. *Acta Petrologica Sinica* 28, 4139–50 (in Chinese).
- Yang F, Ma ZQ, Xu T and Ye S** (1992) A tertiary paleomagnetic stratigraphic profile in Qaidam Basin. *Acta Petrologica Sinica* 13, 97–101 (in Chinese).
- Young GM and Nesbitt HW** (1999) Paleoclimatology and provenance of the glaciogenic Gowganda formation (Paleoproterozoic), Ontario, Canada: a chemostratigraphic approach. *Geological Society of America Bulletin* 111, 264–74.
- Yu DD, Zhang YS, Xing EY, Zuo Z, Hou XH, Wang LL and Zhao WY** (2018) Petrological characteristics and sedimentary environment of the surface mixed rocks in Nanyishan structure, western Qaidam Basin. *Acta Geologica Sinica* 92, 2068–80 (in Chinese).
- Zachos JC, Pagani M, Sloan L, Thomas E and Billups K** (2001) Trends, rhythms, and aberrations in global climate 65 Ma to present. *Science* 292, 686–93.
- Zan JB, Fang XM, Yan MD, Zhang WL and Lu Y** (2015) Lithologic and rock magnetic evidence for the Mid-Miocene Climatic Optimum recorded in the sedimentary archive of the Xining Basin, NE Tibetan Plateau. *Palaeogeography, Palaeoclimatology, Palaeoecology* 431, 6–14.
- Zhang W** (2006) High-resolution Cenozoic magnetostratigraphy in the Qaidam Basin and the Uplift of Tibetan Plateau. Ph.D. thesis, Lanzhou University, Lanzhou, China. Published thesis (in Chinese).
- Zhang XJ, Fan YF, Zhang JJ and Wang GC** (2004) Microelement and geologic significance of Yanchang Formation in Fuxian area, Ordos Basin. *Xinjiang Petroleum Geology* 25, 483–5 (in Chinese).
- Zheng RC and Liu MQ** (1999) Study on paleosalinity of Chang 6 oil reservoir set in Ordos Basin. *Oil & Gas Geology* 20, 22–7 (in Chinese).
- Zheng K, Wu CL, Wei CJ, Gao YH, Guo WF, Chen HJ, Wu D and Gao D** (2019) Geochemistry, zircon U–Pb geochronology and Hf isotopic characteristics for syenogranite and diorite from the western segment of North Altyn. *Acta Petrologica Sinica* 35, 541–57 (in Chinese).
- Zhuang GS, Hourigan JK, Koch PL, Ritts BD and Kent-Corson ML** (2011) Isotopic constraints on intensified aridity in Central Asia around 12 Ma. *Earth and Planetary Science Letters* 312, 152–63.